NASA TECHNICAL REPORT

NASA TR R-141

NASA TR R-141 OTS: 1.75

N64-16005 *

CODE-1

66p.

ON THE HEATING OF THE POLAR UPPER ATMOSPHERE

by Kaichi Maeda

Goddard Space Flight Center

Greenbelt, Maryland

NATIONAL AERONAUTICS AND SPACE ADMINISTRATION • ~~WASHINGTON, D. C.~~ NASA • DECEMBER 1962

ON THE HEATING OF THE POLAR UPPER ATMOSPHERE

By Kaichi Maeda

Goddard Space Flight Center
Greenbelt, Maryland

NATIONAL AERONAUTICS AND SPACE ADMINISTRATION

For sale by the Office of Technical Services, Department of Commerce,
Washington, D.C. 20230 -- Price $1.75

ON THE HEATING OF THE POLAR UPPER ATMOSPHERE

by

Kaichi Maeda

Goddard Space Flight Center

16005

SUMMARY

On the basis of the atmospheric composition given by F. S. Johnson in 1960, the contribution of auroral particles to the dissociation of oxygen molecules in the polar upper atmosphere is investigated. The maximum rate coefficients are 4×10^{-8} $(\mathrm{cm}^3\ \mathrm{sec})^{-1}$ and 2×10^{-8} $(\mathrm{cm}^3\ \mathrm{sec})^{-1}$ for protons of energy spectrum $E^{-2.8}\,dE$ and for electrons of energy spectrum $E^{-4}\,dE$, respectively. The height of maximum dissociation is around 90 km both for protons and electrons. The heating of the polar mesosphere by exothermic association of the oxygen atoms, intensified by the subsidence of the upper polar atmosphere during the polar night, is calculated and found to be close to the estimate given by W. W. Kellogg in 1961. The investigation indicates, however, that Kellogg's estimate should be reduced slightly to allow for the cooling effect produced by far infrared emission from atomic oxygen in the upper atmosphere.

AUTHOR

CONTENTS

ON THE HEATING OF THE POLAR UPPER ATMOSPHERE*

by

Kaichi Maeda
Goddard Space Flight Center

INTRODUCTION

Since air is transparent to the predominant part of the insolation, the atmosphere above the stratosphere is usually considered to be heated directly by the absorption of solar ultraviolet rays by atmospheric oxygen and ozone (Reference 1) whereas the lower atmosphere is warmed mainly from below by the infrared radiation of the earth and by the convection of air. As early as 1951, Bates showed that the earth's upper atmosphere is cooled continuously by far infrared radiation from neutral oxygen atoms. Therefore, it would be natural to assume that in the absence of solar heating the polar upper atmosphere might be cooled in the winter night. Contrary to this assumption, recent meteorological observations have revealed that the polar atmosphere above 60 km is warmer in winter than in summer, although the stratosphere and troposphere are cold (as was expected) except during occasional so-called explosive warming periods (References 2 through 5; also see Figure 13). The presence of a warm mesosphere in the polar night is also confirmed by the synoptic analysis of prevailing easterlies around the 80 km level at high latitudes during the winter (Reference 6).

Moreover, according to direct measurements of upper air density by rocket soundings, the atmospheric temperature in the arctic region near the 200 km level is found to be almost twice that of the temperate latitudes (References 7 and 8), even though the direct comparisons made thus far refer only to the case of summer daytime.** Further evidence for the existence of warm polar upper air is indicated by the study of irregular variations in satellite drag, which are more prominent for satellite orbits passing the polar region (such as Sputnik III, 1959 δ) than for those whose planes are close to the equatorial plane (Vanguard I, 1958 β). Although this difference has not been confirmed

*This work was sponsored in part by the National Science Foundation, Grant NSF/G-13999.

**According to Paetzold (Reference 9) and Karplus et al. (Reference 10), the large value of the ratio of polar air density to that of temperate latitude shown by Horowitz and LaGow (Reference 11) is ascribed to the difference of solar activity corresponding to the period when the measurements were performed.

by recent analysis (Reference 9), the increase of drag is doubtless highly related to solar activity, i.e., the coronal index, the 20 cm solar noise flux (References 12 and 13).

In consideration of these facts, the heating of the polar upper atmosphere by corpuscular radiation was estimated by Krassovsky (Reference 14) and Jastrow (Reference 7). The direct heating of the upper atmosphere by solar corpuscles is also discussed in detail by Ishikawa (Reference 15), although an actual estimate was made only for protons.

Clearly, charged particles impinging on the upper atmosphere lose their energy by ionizing and exciting air-gas constituents along the path of penetration. Part of this energy transferred to the atmosphere will be re-radiated toward outer space; the other part will be converted into thermal energy of the upper atmosphere. Owing to geomagnetic deflections, most charged particles cannot enter the low latitude regions; therefore, corpuscular heating is actually effective only at extremely high altitudes around the auroral zones.

The enormous number of particles trapped by the earth's magnetic field can also be regarded as a large reservoir of corpuscular energy at the top of the atmosphere. In other words, the flux of charged corpuscles scattered in small pitch angles along the geomagnetic lines of force is an additional source of corpuscular heat, corresponding to the *leakage* of trapped particles (Reference 16).

Another important phenomenon in the polar upper atmosphere, called the "abrupt warming of the stratosphere during the polar night," has been found recently (References 4 and 17). This is, however, essentially the same as the so-called "Berlin Phenomenon" discovered by Scherhag in 1952.*

It has been pointed out that these abrupt warmings are connected with the breakdown of the stable polar vortex developed in the shadow of the polar night (References 4 and 19). Also, the time of this breakdown is closely related to solar activity and to geomagnetic activity (Reference 20).

The fact that these sharp increases of stratospheric temperature are observed within the dark shadow of the polar night, and are known to have occurred within a day or so after the maximum of a given solar event (References 4 and 19), leads to speculation that such irregular abrupt warmings are caused indirectly by solar corpuscles.** Since the corpuscular heating is effective only above the mesosphere and in the vicinity of the auroral zones, the possible mechanism of energy transfer from the upper part of the auroral zone to the deep polar stratosphere, as well as to the stable warm mesosphere in the

*The variations of aerological situations in these phenomena were investigated in detail recently by Scherhag (Reference 18), with regard to the events which occurred in the winter of 1958. The author wishes to express his appreciation to him for data and notes on these events and a similar event which occurred at the end of 1960.

**This irregular warming of polar atmosphere should be distinguished from that corresponding to the usual breakdown of the cold polar vortex, which, incited by sunlight, occurs after the equinox.

polar night, needs to be clarified. An understanding of this mechanism might also provide some valuable clues for seasonal weather forecasting.

An important role of oxygen in the upper atmosphere has been noted by Kellogg (Reference 6). Although he ruled out the *direct* heating of the polar upper atmosphere by auroral particles, the contribution of these particles to the dissociation of oxygen molecules, and the subsequent heating of the atmosphere by their re-association, cannot be ignored. That is, oxygen molecules in the upper atmosphere may be dissociated into atoms through bombardment by auroral particles; and the dissociated oxygen, following the general circulation of the earth's atmosphere, subsides towards the polar region. With the increased pressure resulting from subsidence, the collision frequency increases rapidly and some atomic pairs again form molecules and release the excess molecular binding energy. This released energy must be dissipated into the atmosphere as thermal energy. In these processes of upper air heating, the role of oxygen is therefore that of a catalyst in chemical reactions, and the mechanism of energy release is quite analogous, as was pointed out by Kellogg (Reference 6), to the release of the latent heat of condensation of water vapor in the atmosphere.

Since the rate of energy release by the association of atomic oxygen is approximately proportional to the cube of the air pressure, a very steep increase of temperature in the stratosphere can be expected from this subsidence of atomic oxygen. One of the main purposes of this paper is to indicate the effect auroral particles have on the polar upper atmosphere in the production of atomic oxygen.* Solar ultraviolet radiation, which is regarded as a major source of oxygen dissociation in the middle and lower latitudes, may no longer predominate in the polar mesosphere in winter; and the continuous supply of oxygen atoms caused by the effects of auroral particles can be an important source of heating of the polar upper air.

FLUX OF SPIRALING PARTICLES IN THE POLAR ATMOSPHERE

Since the flux of cosmic rays which penetrate the atmosphere to the ground is negligible as compared with that of so-called auroral particles in the polar regions, we shall consider only the contribution of auroral particles, which may be regarded as consisting of non-relativistic protons and electrons.

The magnetic field in the polar regions may be regarded as uniform and vertical to the earth's surface. In these regions charged particles impinging into the atmosphere follow a spiral orbit along the magnetic line of force. The direct evidence of spiral

*The symbols used in this discussion are presented in Appendix A.

motion of auroral protons is shown by Meinel (Reference 21), who obtained the two types of Doppler shift of the hydrogen alpha line—one corresponding to the parallel component of impinging velocity of protons along the line of force (asymmetric broadening), and the other corresponding to the normal component to the line of force (symmetric broadening). Since the rates of energy loss of these particles are the same in all directions, the pitch angle, α, of a particle is constant throughout its range (Reference 22). More specifically, incident particles maintain spiral motions with constant pitch angles, while the radius of gyration decreases correspondingly with the energy loss experienced by the particle at increasing atmospheric depths.

Regarding the constancy of pitch angle of the spiraling particles through the atmosphere, Singer (Reference 23) suggested estimating the intensity of the non-relativistic particles in the upper atmosphere by using Liouville's theorem. However, the application of Liouville's theorem can be extended only to the particles of constant ionization loss, and not to the particles whose rates of energy loss change with their energy (see Appendix B).

The intensity of spiraling low energy particles, whose rates of energy loss increase rapidly with the decrease of their energies, can be estimated by means of the so-called Gross transformation (Reference 24), which must be modified as will be shown in the following discussion. Since scattering is dominant for low energy electrons, the same method cannot be used for auroral electrons.

Low Energy Protons

Range-Energy Relation in Air

As can be seen in Figure 1, the rate of energy loss E of protons per unit depth of air R can be approximated, below a certain energy value E_u, by the equation

$$-\frac{dE}{dR} = AE^{-m}, \tag{1}$$

with the experimental data given by Segrè (Reference 25), where A and m are given in Table 1. There is also a lower limit of energy, E_ℓ, for Equation (1) to be valid, but the contribution below this limit to the total range is negligible.

Several direct observations show that the energy spectrum of auroral protons can be expressed by

$$j(E)\,dE = \alpha E^{-n}\,dE, \qquad n > 0, \tag{2}$$

where $n = 5.5$ according to direct measurements by a rocket borne detector (Reference 25).

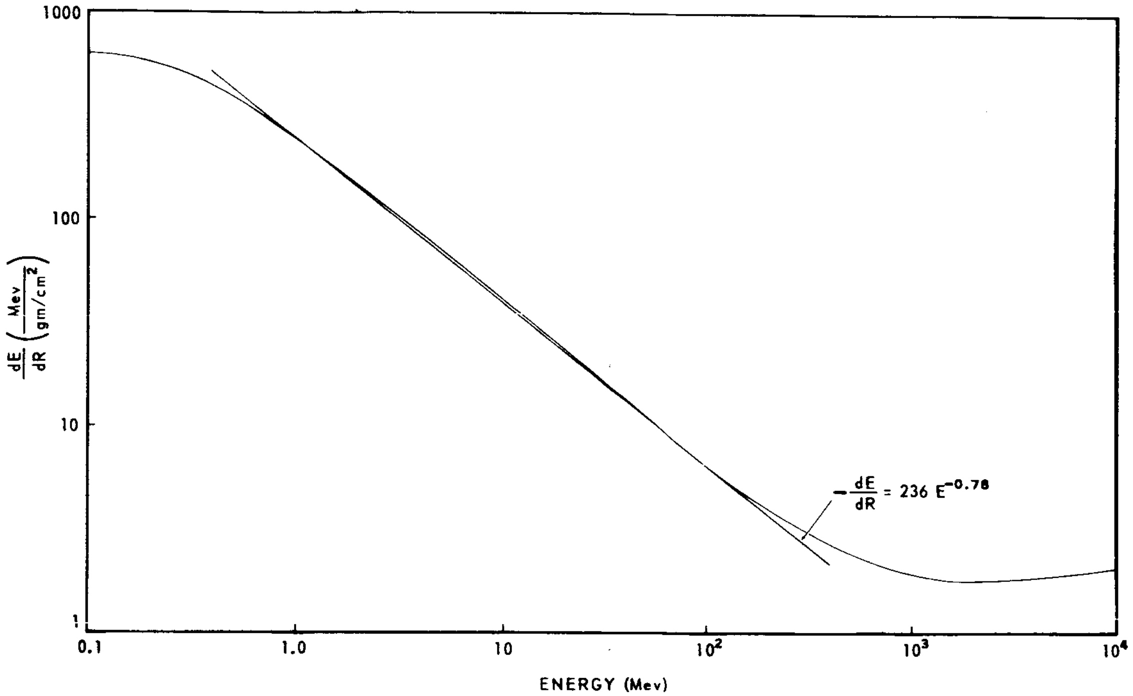

Figure 1 - Rate of energy loss of protons in air (below the minimum ionization loss) as a function of the energy

Table 1

Energy Loss Coefficients in Air

Particle	A	m	E_u	E_ℓ
Proton*	236	0.78	300 Mev	400 kev
Electron**	0.38	0.96	100 kev	4 kev

*Based on Segrè's data (Reference 26)
**Based on Katz and Penfold's data (Reference 27)

Since a simple relationship exists between the range of a particle at an atmospheric depth x (in gm/cm^2), and the energy of the particle at another depth x', it is convenient to convert the energy spectrum into a range spectrum. It follows from Equation 1 that

$$R = \int_0^E \frac{dE'}{AE'^{-m}} = \frac{1}{A}\frac{E^{m+1}}{m+1} \qquad (3)$$

$$E = \left[RA(m+1)\right]^{\frac{1}{m+1}}.$$

Combining Equations 1, 2, and 3, we get

$$j(R)\,dR = kR^{-\ell}dR , \tag{4}$$

where

$$k = \alpha A^{-\frac{n-1}{m+1}} (m+1)^{-\ell} \quad \text{and} \quad \ell = \frac{n+m}{m+1} .$$

The numerical relation between n and ℓ is presented in Table 2.

Table 2
The Numerical Relation
Between n and ℓ

ℓ	n (Proton)	n (Electron)
1.00	1.00	1.00
2.00	2.78	2.96
2.53	3.73	4.00
2.68	4.00	4.29
3.00	4.56	4.92
3.53	5.50	5.95

Total Intensity of Spiraling Protons

The distribution of auroral protons beyond the earth's atmosphere can be regarded as isotropic; thus the total flux at the top of the atmosphere is

$$I_o = 2\pi \int_{R_0}^{R_m} j(R)\,dR , \tag{5}$$

where R_o is the threshold range set by the detector. By Equation 4, the above expression becomes

$$I_o = \begin{cases} 2\pi k \ln \dfrac{R_m}{R_o} , & \text{for } \ell = 1, \\ \dfrac{2\pi k}{\ell-1} \dfrac{1}{R_o^{\ell-1}} \left[1 - \left(\dfrac{R_o}{R_m}\right)^{\ell-1} \right] & \text{for } \ell > 1. \end{cases} \tag{6}$$

Since we can assume that $R_m = \infty$ for $\ell > 1$, Equation 6 becomes

$$I_o = \frac{2\pi k}{\ell-1} R_o^{-(\ell-1)} .$$

The directional intensity of the flux at a depth x and at a pitch angle α is

$$j(x,\alpha) = \int_{(R_o+y)}^{R_m} k R^{-\ell} dR , \tag{7}$$

where $y = x/\cos\alpha$, the actual path length traversed by the protons in reaching the depth x. The directional integral intensity, therefore, is

$$j(x,\alpha) = \begin{cases} k \ln\left(\dfrac{R_m}{R_o + y}\right), & \text{for } \ell = 1, \\ \dfrac{k}{\ell - 1} \dfrac{1}{(R_o + y)^{\ell - 1}} \left[1 - \left(\dfrac{R_o + y}{R_m}\right)^{\ell - 1}\right], & \text{for } \ell > 1. \end{cases} \quad (8)$$

For $\ell > 1$ and $R_m = \infty$, the second expression of Equation 8 becomes

$$j(x,\alpha) = j(y) = \frac{k}{\ell - 1} (R_o + y)^{-\ell + 1} .$$

Therefore the total flux $I(x)$ at the depth x is

$$\begin{aligned} I(x) &= 2\pi \int_0^{\frac{\pi}{2}} j(x,\alpha) \sin\alpha \, dx \\ &= 2\pi x \int_x^{\infty} j(y) \frac{dy}{y^2} . \end{aligned} \quad (9)$$

From Equations 5, 7, and 9, we finally obtain

$$\frac{I(x)}{I_o} = \begin{cases} 1 - F_o(\xi) & \text{for } \ell = 1, \\ 1 - F_{\ell - 1}(\xi) & \text{for } \ell > 1, \end{cases}$$

where $\xi = x/R_o$;

$$F_o(\xi) = \frac{1}{\ln \dfrac{R_m}{R_o}} \left[\ln(1 + \xi) + \xi \ln\left(1 + \frac{1}{\xi}\right)\right] \quad \text{for } \ell = 1;$$

and

$$F_{\ell - 1}(\xi) = (\ell - 1)\xi \ln\left(1 + \frac{1}{\xi}\right) - \xi \sum_{r=2}^{\ell - 1} \frac{(-1)^r}{r - 2} ({}_{\ell - 1}C_r)\left[1 - \left(1 + \frac{1}{\xi}\right)^{-(r-1)}\right] \quad \text{for } \ell > 1. \quad (10)$$

In Equation 10, R_m is taken as ∞, and

$${}_{\ell - 1}C_r = \frac{(\ell - 1)!}{(\ell - 1 - r)!\,r!} .$$

From Figure 2, it is seen that the maximum penetration depth depends on the upper limit of energy spectrum, while the rate of decrease of the flux in the atmosphere depends on the cutoff energy of the measuring instrument. It should be noticed that the spiraling flux becomes zero below a certain depth, which corresponds to the upper limit of the range spectrum R_m for vertical incidence. However, there is not a sharp decrease

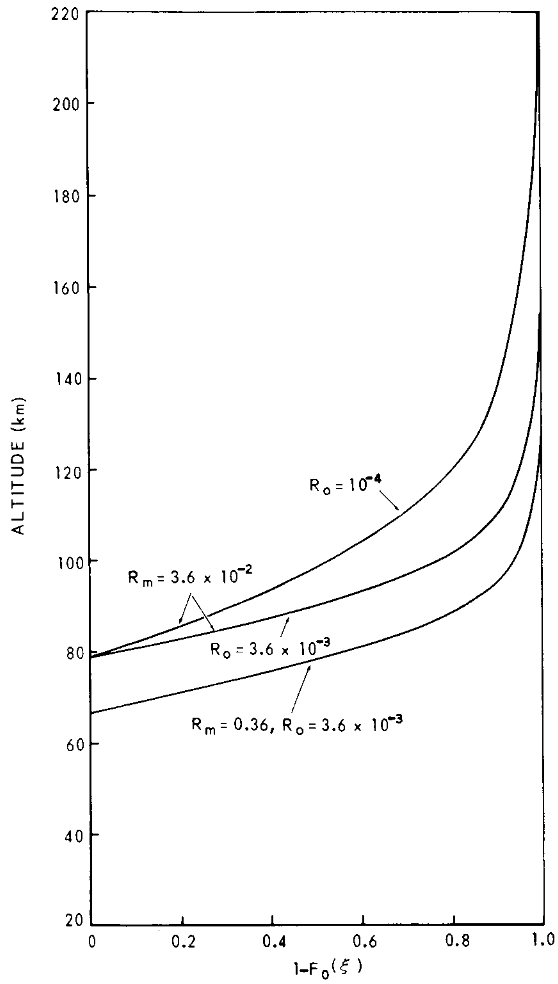

Figure 2 - Relative total intensity of spiraling protons $I(z)/I_0$ versus altitude z for the case $\ell = 1$, where the ranges R = 0.36, 3.6 x 10 $^{-2}$, 3.6 x 10^{-3} and 10^{-4} correspond to the energies E, 12, 5, 1.2, and 0.065 (in Mev), respectively

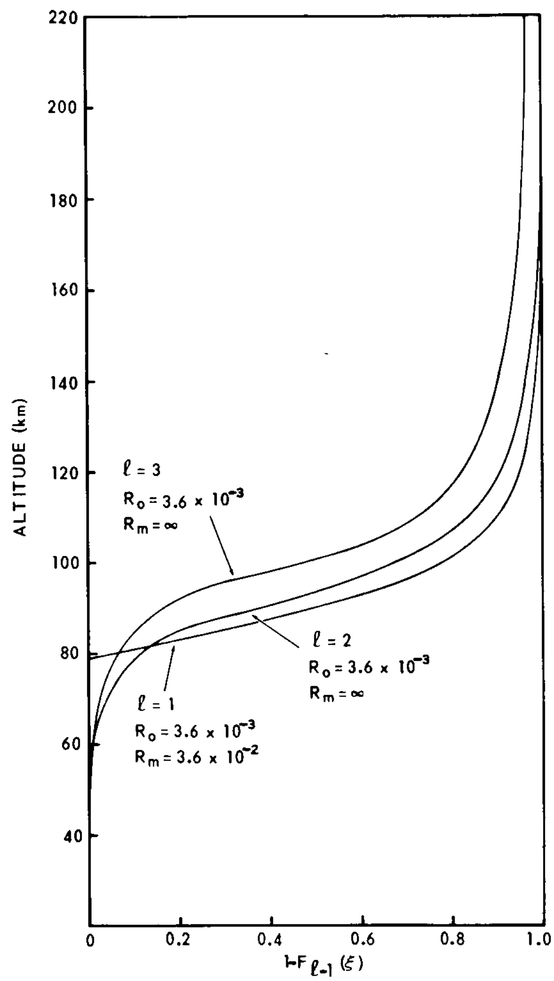

Figure 3 - Relative total intensity of spiraling protons $I(z)/I_0$ as a function of altitude z for the cases ℓ = 1, 2, and 3

of total flux for the case of $R_m = \infty$ (Figure 3, in which a comparison is made for the cases of $\ell = 1$ with $R_m = 3.6 \times 10^{-2}$, and $\ell = 2$ and 3 with $R_m = \infty$). It should be also noted that—even for the same cutoff and upper limit of spectra—the rate of decrease of total intensity with atmospheric depth becomes steeper for the steeper spectrum, i.e., for the larger value of ℓ.

In these figures, the expression $I(x)/I_0$ is transformed into $I(z)/I_0$ (where z is the altitude of the level of atmospheric depth x) by making use of the relation between the atmospheric depth x (gm/cm^2) and the altitude z (km). The following atmospheric model was used to derive $I(z)/I_0$:

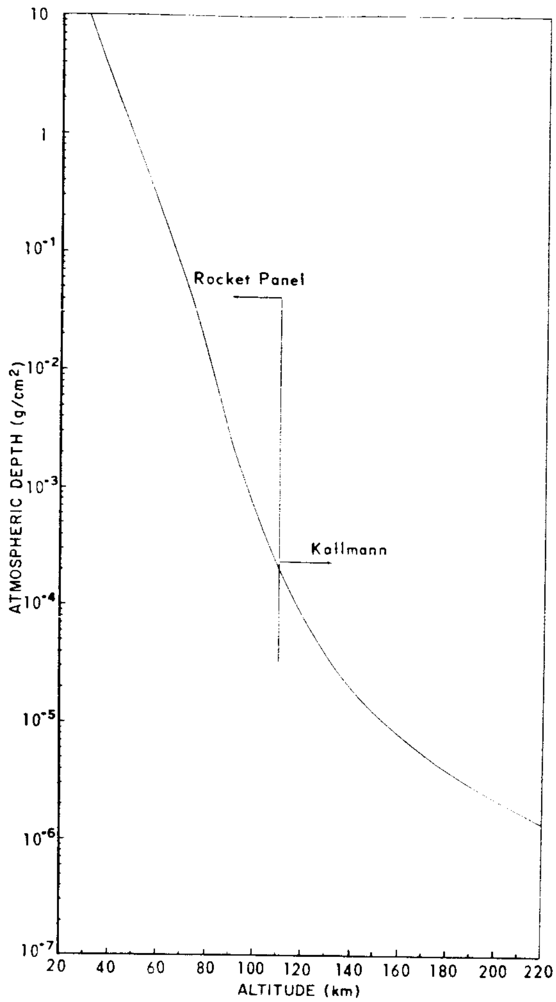

Figure 4 - Atmospheric depth as a function of altitude. The atmospheric model is taken from Rocket Panel data for $z \leq 110$ km, and from Kallmann's table for $110 < z \leq 400$ km.

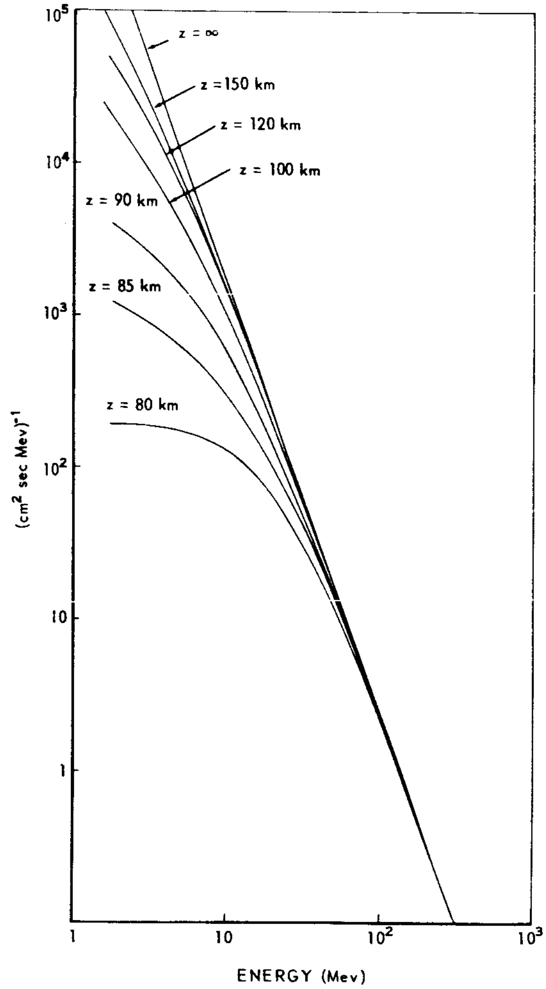

Figure 5 - Omnidirectional differential energy spectra of spiraling protons $i_z(E)$ with an arbitrary scale

$z \leq 110$ km Rocket Panel Data (Reference 28), $110 \leq z \leq 400$ km Kallmann's Table (Reference 29), $z > 400$ km King-Hele (Reference 30).

The x-z curve based on this atmospheric model is shown in Figure 4.

Omnidirectional Differential Spectra

Since the rate of energy loss of penetrating protons in the atmosphere is larger for the protons of lower energy (below minimum ionization), the flux of low energy protons decreases faster than that of high energy protons. Therefore, the form of the differential energy spectrum changes with the atmospheric depth. To illustrate this, we shall compute the change of range spectrum of low energy protons penetrating the atmosphere.

The omnidirectional differential range spectrum at the top of the atmosphere is given by

$$i_o(R)\,dR = 2\pi\, j(R)\, dR\,;$$

and at the depth x,

$$i_x(R)\,dR = 2\pi \int_0^{\pi/2} j\left(R + \frac{x}{\cos\alpha}\right) \sin\alpha\, d\alpha\,.$$

For the case of $j(R)\,dR = k R^{-\ell} dR$, setting $\cos\alpha = \mu$, and $x/R = \eta$,

$$i_x(R)\,dR = 2\pi k R^{-\ell}\, dR \int_0^1 \left(1 + \frac{\eta}{\mu}\right)^{-\ell} d\mu\,.$$

Finally, for the particular case $\ell = 2$, we obtain,

$$i_x(R) = \left[\frac{1 + 2\eta}{1 + \eta} - 2\eta \ln(1 - \eta)\right] i_o(R). \quad (11) \tag{11}$$

Using the energy-range relation of protons and the x-z curve, the corresponding omnidirectional differential energy spectra, $i_z(E)$, are shown for several altitudes in Figure 5. From this the effective power of the spectrum is seen to decrease with the atmospheric depth x (that is, with the altitude z).

Directional Intensity

Owing to their spiral motions in the atmosphere, the intensity of obliquely penetrating protons decreases more rapidly than that of vertically incident protons. Therefore, even if the distribution of incident protons beyond the earth's atmosphere is assumed to be isotropic, the zenith angle distribution of proton flux becomes steeper with increasing atmospheric depth. For the case of $\ell > 1$, with $R_m = \infty$, the change of the zenith angle distribution of slow protons can be shown as follows: Since the incident proton flux can be assumed to be isotropic, the directional intensity of slow protons above the atmosphere is given from Equation 5:

$$j(o) = \frac{I_o}{2\pi} = \frac{k}{\ell - 1} R_o^{-(\ell - 1)}$$

The directional intensity at the atmospheric depth x is given by Equation 7; therefore, the directional relative intensity is

$$\frac{j(y)}{j(o)} = \left(1 + \frac{y}{R_o}\right)^{-(\ell-1)} , \tag{12}$$

where

$$y = \frac{x}{R_o \cos \alpha} .$$

The numerical values of Equation 12 are shown in Figure 6 for the case $\ell = 2$ with $R_o = 3.6 \times 10^{-3}$ gm/cm^2 ($E_o \approx 1.2$ Mev). From this figure it is seen that the flux of slow protons converges towards the vertical direction (which is also the direction of the magnetic line of force) with increasing atmospheric depth. Equation 12 also shows that the steeper the spectrum (i.e., the larger the value of ℓ) the steeper the zenith angle distribution at a certain depth in the atmosphere. However, the above calculations are based on the assumption of a flat atmosphere. If the effect of the curvature of the atmospheric layer is taken into account, the decrease of the obliquely incident proton flux must be less steep at large zenith angle (>80°) than that shown by Equation 12 and Figure 6.

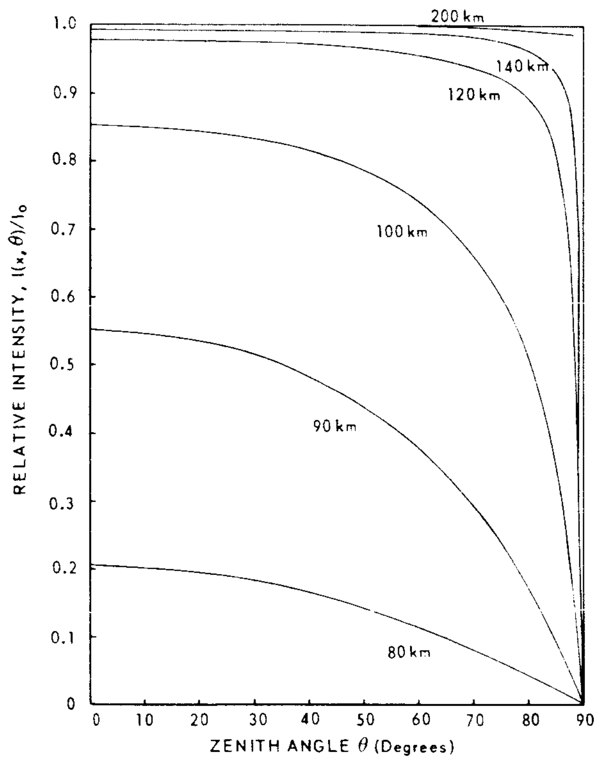

Figure 6 - Zenith angle distributions of spiraling protons in the protons in the atmosphere for the case $\ell = 2$, $R_m = \infty$, and $R_o = 3.6 \times 10^{-3}$ gm/cm^2 ($E_o \approx 1.2$ Mev)

Auroral Electrons

As has been previously mentioned, the majority of incoming particles in severe aurorae are protons with energies less than several hundred kev, following spiral orbits around magnetic field lines from outer space to the earth's atmosphere. Although the incoming protons with energies around several hundred kev are indicated by the observation of Doppler-shifted Balmer lines in the auroral spectrum, it is found (Reference 25) that the major fraction of auroral particles in weak aurorae consist of electrons with energies below 50 kev (according to direct measurements with the aid of a rocket borne detector). The integral energy spectrum is about 4×10^{10} E^{-3}/cm^2-sec-sterad, where

E is expressed in kev.* Air glows and weak aurorae are observed within the auroral zone almost every clear night. Although the auroral zones are located slightly higher in geomagnetic latitude (~70°) than that of the so-called "horn" of the outer Van Allen belt (~60°), it is probable that the leakage of the geomagnetically trapped electrons from the outer magnetosphere around the earth is one of the important sources of these auroral electrons.

Practical Range of Electrons in Air

The rate of energy loss, $-dE/dR$, is given theoretically by Bethe (Reference 31):

$$R = \int_0^E \frac{dE}{-\frac{dE}{dR}} .$$

Because of the multiple Coulomb scattering and straggling effects, both of which are predominant for the low energy electrons travelling through the air, the rate of energy loss given by Bethe's formula is inadequate for calculating the residual range of low energy electrons.

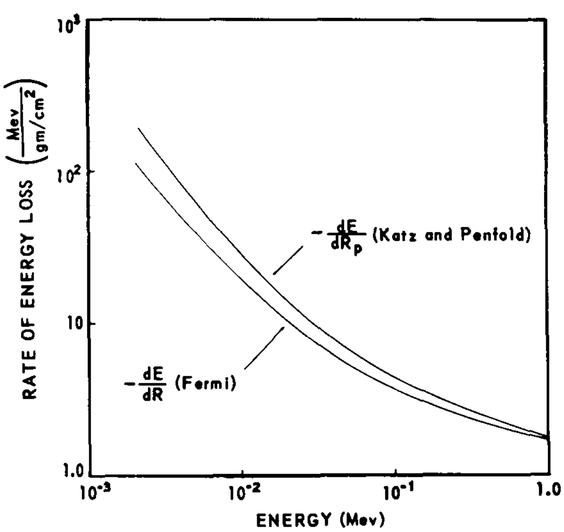

Figure 7 - Rate of energy loss of electrons in air in terms of the true range R and of the practical range R_p as a function of electron energy

On the other hand, the practical range R_p, which is the projected depth of the incident electrons in the initial direction, has been defined and is experimentally measurable (Reference 27). Since the theoretical range R is the total length measured along the tortuous path of an electron in the air (Reference 32), the practical range R_p is always shorter than R. A comparison of the rate of energy loss in terms of R_p and of R is shown in Figure 7. From this figure, it is apparent that the difference between dE/dR_p and dE/dR increases with decreasing electron energy, because multiple scattering increases at low energies. The coefficients A and m in Table 1 indicate an empirical approximation of $-dE/dR_p$ by Equation 1 with E given in Mev.

*Originally, the observed data were approximated by $2.5 \times 10^9 e^{-E/5}$ (E in kev) for the energy range between 3 and 30 kev. In this energy interval, both expressions agree within the accuracy of the measurements.

The angular distribution of the scattered electrons under the multiple Coulomb scattering is known to be approximately Gaussian. However, if the penetration depth of electrons is far larger than the mean free path of Coulomb scattering of electrons in the air, λ_c, the distribution is no longer Gaussian but is of the form $\cos^2\theta$, where θ is the scattering angle (Reference 33).

The corresponding mean angle of scattering is around 30 degrees and remains the same with further increase of thickness. In other words, the penetration of electron flux deeper than λ_c in the air can almost be regarded as diffusion.

Concerning the diffusion of electrons in the atmosphere, there is another factor named "back diffusion thickness," x_d, beyond which the backscattered electron is saturated. If the penetration depth of electrons exceeds x_d, complete diffusion of electrons starts. However, in air the ratio of the number of backscattered electrons to that of incident primary electrons at saturation (back diffusion coefficient) is less than 0.2. Therefore, the integral flux of auroral electrons in the upper atmosphere, obtained by the integration of attenuation curves of differential flux, should be multiplied by a factor 1.2, below x_d for the lowest energy of incident electrons.

In Figure 8, λ_c, x_d and R_p are presented as functions of the incident electron energy. λ_c is computed by

$$\lambda_c \approx \frac{A_a}{\sigma_c N},$$

where A_a is the effective atomic weight of air nuclei (14.78), N is Avogadro's number (6.024×10^{23}), and σ_c is the total cross section of Coulomb scattering. x_d is estimated from experimental data on aluminum, multiplied by a reducing factor 0.34, which is approximately the ratio of the total cross section of Coulomb scattering. σ_c is derived in Appendix C as a function of the energy of incident electrons.

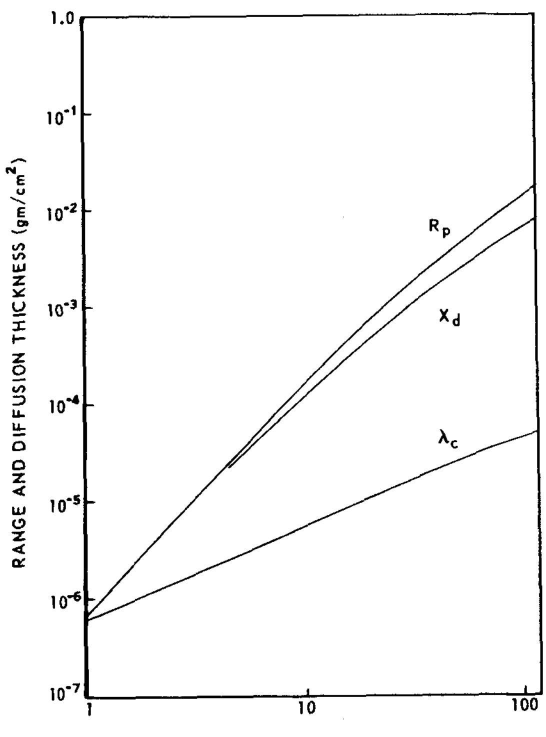

Figure 8 - Practical range R_p, back diffusion thickness x_d, and the mean free path for Coulomb scattering λ_c, of electrons in air as functions of electron energy E

Absorption of Electrons in Air

As we have seen earlier, the penetration of electrons in air beyond the depth of several times λ_c, can be regarded

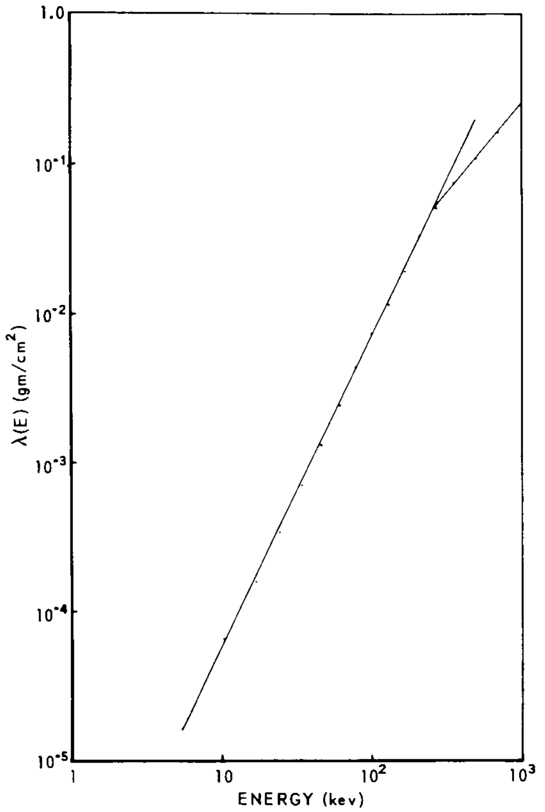

Figure 9 - Attenuation mean free path of electrons in air as a function of incident electron energy

approximately as diffusion. This is due to the multiple Coulomb scattering and the straggling effect caused by frequent large fractional energy transfers in electron-electron inelastic collisions in the air. Thus, even if the incident electron flux is monoenergetic, the energy of the electrons at a certain depth is no longer monochromatic but spread widely toward the lower energies, and the electrons of lowest energy, having lost a large fraction of initial energy, are captured by air nuclei. Consequently, the intensity of auroral electrons in the atmosphere decreases gradually with atmospheric depth.

The rate of decrease of electron flux per unit atmospheric depth is a function of the energy of the incident electrons. This has been observed in several laboratory experiments (References 34-39). According to these measurements, the differential intensity of electrons with initial energy E, at the depth (air thickness) x is approximately

$$j(E,x)\,dE = j_0(E)\,e^{-x/\lambda(E)}\,dE\,,$$

where $j_0(E) = j(E,0)$, the initial differential intensity of electrons with a kinetic energy of E; and $\lambda(E)$, which can be called the "attenuation mean free path of electrons in the air," is the inverse of the mass absorption coefficient of electrons with initial energy E.

Figure 9 shows $\lambda(E)$ as a function of the initial energy of electrons, derived from the experimental results obtained by Lenard (Reference 34), Schmidt (Reference 37), and Friman (Reference 39), and summarized into a table by Bothe (Reference 40). It is evident from Figure 9 that the attenuation mean free path of electrons with initial energy E can be expressed empirically by

$$\lambda(E) = bE^{m'}, \tag{13}$$

where the numerical values of the constants b and m' are given in Table 3.

Although the power m' decreases significantly above the energy about 300 kev—from 2.2 to 1.33, we shall use $m' = 2.2$ for all energy ranges above 5 kev. Since the intensity of high energy electrons is very small owing to the sharp drop of energy spectrum on high energy side, the use of $m' = 2.2$ in Equation 13 beyond 300 kev does not introduce any serious errors into future computations.

Table 3
Constants of Attenuation
Mean Free Path, $\lambda(E)$

b	m'	Energy Range
3.15×10^{-7} (E in kev) 1.26 (E in Mev)	2.2	5 kev < E < 300 kev
2.94×10^{-5} (E in kev) 0.29 (E in Mev)	1.33	0.3 Mev < E < 3 Mev

Total Intensity of Auroral Electrons

The attenuation of electron intensity in the air is approximately exponential; therefore, the differential intensity of electrons entering into the upper atmosphere at pitch angle α with respect to the vertical magnetic field, at the atmospheric depth x, can be written:

$$j(E,x,\alpha)\,dE = j_0(E)\exp\left[-\frac{x}{\lambda(E)\cos\alpha}\right], \tag{14}$$

where $j_0(E)$ is the differential energy spectrum of incident electrons; and $\lambda(E)$, the attenuation mean free path of electrons, is given by the empirical formula (Equation 13) (see also Figure 9 and Table 3). Thus the total flux at the depth x becomes

$$I(x) = 2\pi\int_0^{\frac{\pi}{2}}\int_{E_0}^{\infty} j_0(E)\exp\left[-\frac{x}{\lambda(E)\cos\alpha}\right]\sin\alpha\,d\alpha\,dE. \tag{15}$$

The initial differential energy spectrum $j_0(E)$ can be assumed as in Equation 2, where $n = 4$, according to the direct measurements by McIlwain (Reference 25). Then the integral in the right side of Equation 15 can be written:

$$I(x) = 2\pi x\int_{E_0}^{\infty} j_0(E)\int_x^{\infty} e^{-y/\lambda(E)}\,y^{-2}\,dy\,dE. \tag{16}$$

By substituting $t = 1/\lambda(E) = E^{-m'}/b$ into Equation 16, we have

$$I(x) = \frac{2\pi a}{m'}\,b^{\beta}\int_0^{\frac{1}{\lambda_0}} t^{\beta-1}G(tx)\,dt\ ,$$

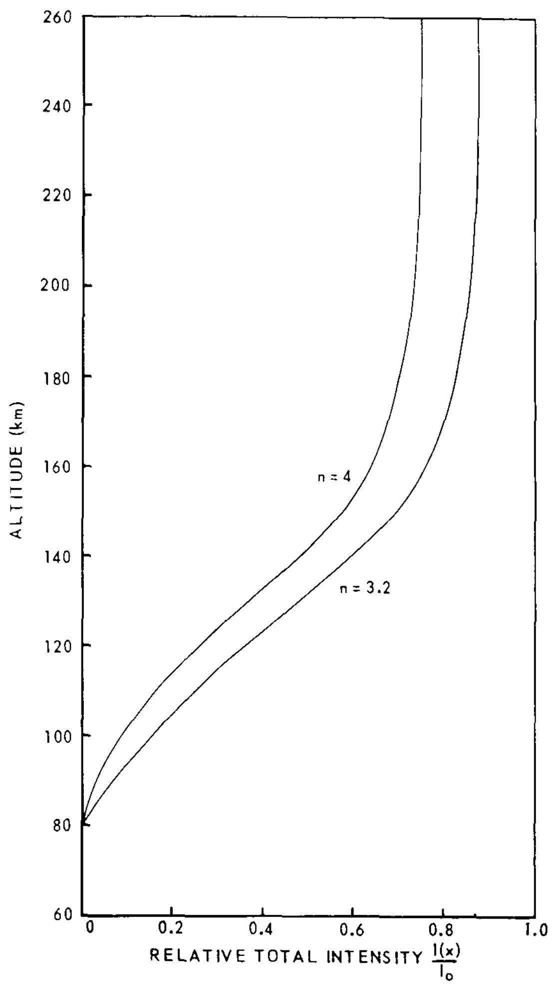

Figure 10 - Relative total intensities of spiraling electrons for two different energy spectra as functions of altitude

where

$$G(u) = \int_1^{\infty} \frac{e^{-us}}{s^2}\, ds = u \int_u^{\infty} \frac{e^{-s}}{s^2}\, ds .$$

and $G(tx)$ is called the Gold integral (Reference 24), which is defined by

$$\beta = \frac{(n-1)}{m'}, \quad \text{and} \quad \lambda_o = \lambda(E_o) = b E_o^{m'},$$

The initial total intensity of auroral electrons is given by letting $x = 0$ in Equation 15:

$$I_o = \frac{2\pi a}{m'} b^{\beta} \frac{\lambda_o^{-\beta}}{\beta} .$$

Therefore, the relative total intensity at the depth x, is

$$\frac{I(x)}{I_o} = \beta \lambda_o^{\beta} \int_0^{\frac{1}{\lambda_o}} t^{\beta - 1} G(tx)\, dt .$$

The two curves in Figure 10 represent $I(x)/I_o$ for $n = 4$ ($\beta = 1.363$) and $n = 3.2$ ($\beta = 1$) with $E_o = 10$ kev. By comparing Figure 10 with Figures 2 and 3, it can be seen that the decrease of electron flux in the upper atmosphere is not so steep as that of the protons in both cases for the value of n.

Omnidirectional Differential Spectra

Since the attenuation of electron flux is larger for the electrons of lower energies, the energy spectrum of electrons changes with atmospheric depth. To see this variation, we calculate the omnidirectional differential energy spectra of electrons at the atmospheric depth x as follows:

$$i_x(E)\, dE = 2\pi \int_0^{\pi/2} j(E) \exp\left[- \frac{x}{\lambda(E)} \cos a\right] \sin a\, da\, dE ,$$

which by the Gross transformation, becomes

$$i_x(E)\,dE = 2\pi a E^{-n} x \int_x^{\infty} y^{-2} e^{-y/\lambda(E)} dy\, dE.$$

Since the omnidirectional differential intensity at the top of the atmosphere is given by

$$i_o(E)\,dE = 2\pi j_o(E)\,dE\,,$$

$$i_x(E) = i_o(E)\, G\left(\frac{x}{\lambda(E)}\right),$$

where $\lambda(E)$ is given by Equation 13. For large values of $x/\lambda(E)$, the Gold integral of the omnidirectional differential intensity at the top of the atmosphere can be approximated by (Reference 24, p. 440)

$$\frac{i_x(E)}{i_o(E)} \approx \frac{e^{-\frac{x}{\lambda(E)}}}{\frac{x}{\lambda(E)}}.$$

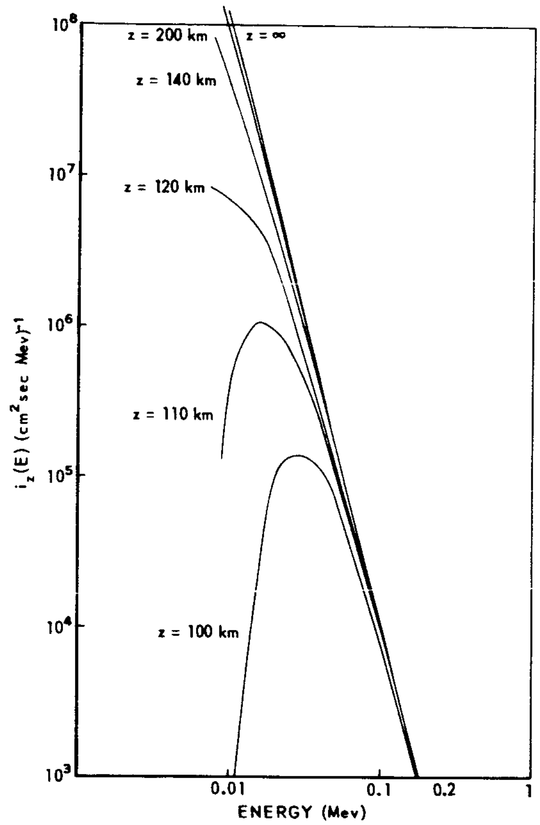

Figure 11 - Omnidirectional differential spectra of auroral electrons with an arbitrary scale at different altitudes for n = 4

By using the x-z curve shown in Figure 4, the $i_x(E)$'s are easily transformed into the $i_z(E)$'s shown in Figure 11, from which the intensity of the low energy side of the spectrum is seen to decrease very rapidly. Owing to this rapid decrease, the sharp edge of lowest energy of the initial spectrum becomes a round peak with increasing atmospheric depth; and the position of this peak shifts towards the high energy side with increasing atmospheric depth.

Directional Intensity

Although most of the impinging electrons in the upper atmosphere can be regarded as being diffused through the air, the attenuation is smallest for electrons travelling in a vertical direction, in which the line of force of the earth's magnetic field is also parallel (i.e., the larger the zenith angle, the larger the attenuation).

The dependence of the integral electron intensity in the upper atmosphere on the zenith angle can be illustrated by integrating the directional differential intensity of auroral electrons given by Equation 14 with respect to energy E. This yields the directional integral intensity of electrons at the atmospheric depth x:

$$J_x(>E_o, \alpha) = \int_{E_o}^{\infty} j(E, x, \alpha)\, dE$$

$$= \frac{a}{m'} \left(\frac{b}{y}\right)^{\beta} \int_0^{\frac{y}{\lambda_o}} e^{-v} v^{-1}\, dv ,$$

where $\lambda_o = \lambda(E_o)$, $y = x/\cos\alpha$ and $v = y/\lambda(E)$. The initial directional integral flux is

$$J_o(>E_o) = \int_{E_o}^{\infty} j_o(E)\, dE$$

$$= \frac{a}{m'} \left(\frac{b}{\lambda_o}\right)^{\beta} \frac{1}{\beta} .$$

Therefore the relative variations of directional integral intensity of electrons at the atmospheric depth x is

$$\frac{J_x(>E_o, \alpha)}{J_o(>E_o)} = \left(\frac{\lambda_o}{y}\right)^{\beta} \beta\, \Gamma_{y/\lambda_o}(\beta) , \tag{17}$$

where $\Gamma_{y/\lambda_o}(\beta)$ is the incomplete Gamma function defined by

$$\Gamma_t(n) = \int_0^{t} e^{-v} v^{n-1}\, dv .$$

The evaluations of Equation 17 are done numerically by using the table of incomplete Gamma functions (Reference 41). By using the x-z curves of Figure 4, the relative integral intensities given by Equation 17 are transformed into $J_z(>E_o, \alpha)/J_o(>E_o)$. The results are shown in Figure 12 for several altitudes. It is interesting to note that the dependence of the total intensity on the zenith angle becomes steeper with increasing depth, approaching the form $\cos^2\alpha$ at about 120 km, and that it again becomes isotropic with increasing atmospheric depth. The foregoing calculations, however, are based on a flat atmosphere. Therefore, the intensity of electrons at large zenith angle (>80°) is underestimated, i.e., if the curvature of the atmosphere is taken into account, the intensity of electrons travelling obliquely with very large zenith angles (>80°) is not as small as that shown in Figure 12.

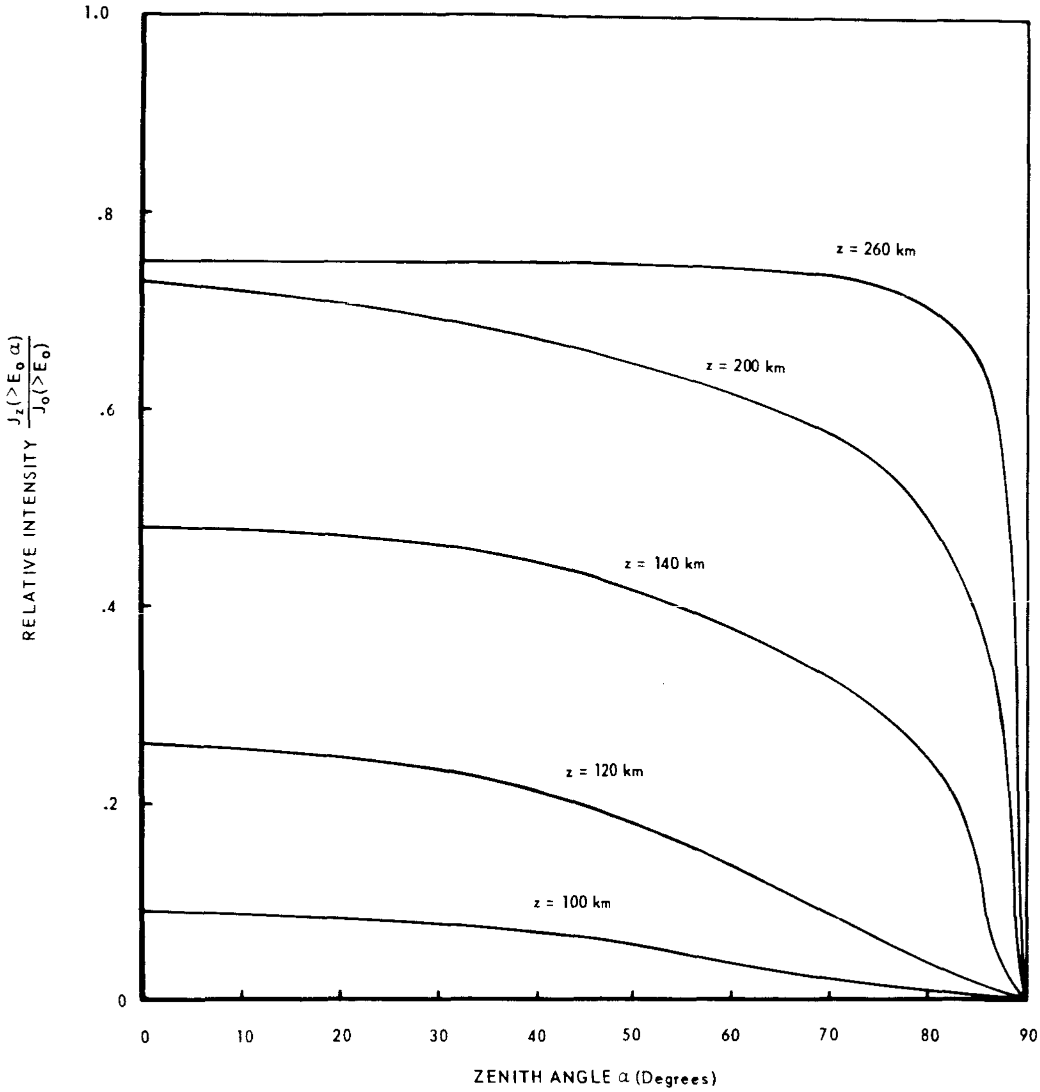

Figure 12 - Relative integral intensity of auroral electrons as a function of zenith angle, $n = 4$

STRUCTURE OF THE POLAR ATMOSPHERE

The primary properties of the atmosphere are density, temperature, pressure, composition and motion. Several names are given to the regions of the atmosphere according to composition: ozonosphere, ionosphere, or hemosphere, and heterosphere (Reference 42). However, owing to the remarkable change with altitude, atmospheric temperature is one of the most common quantities used for investigating the earth's atmospheric structure. The atmospheric regions are also named according to the different temperature gradients in these regions from the earth's surface outward: troposphere, stratosphere, mesosphere, thermosphere and exosphere. The transient levels between these regions are called tropopause, stratopause, mesopause and thermopause, respectively.

Atmospheric Temperature and its Time Variations

The vertical distributions of atmospheric temperature at three different latitudes—corresponding to the polar, temperate and tropical zones—are shown in Figure 13 (References 2, 3, 5, and 6). The heights and temperatures of these levels change with the seasons and differ with the latitudes. These variations in the polar atmosphere are presented in Table 4. Both Table 4 and Figure 13 show the very large temperature difference between summer and winter in the polar mesopause. This fact was recently confirmed by Quiroz (Reference 43) who showed that the arctic air density was low above 65 km in winter, while in the middle and tropical latitudes the air density above this level is slightly higher in winter.

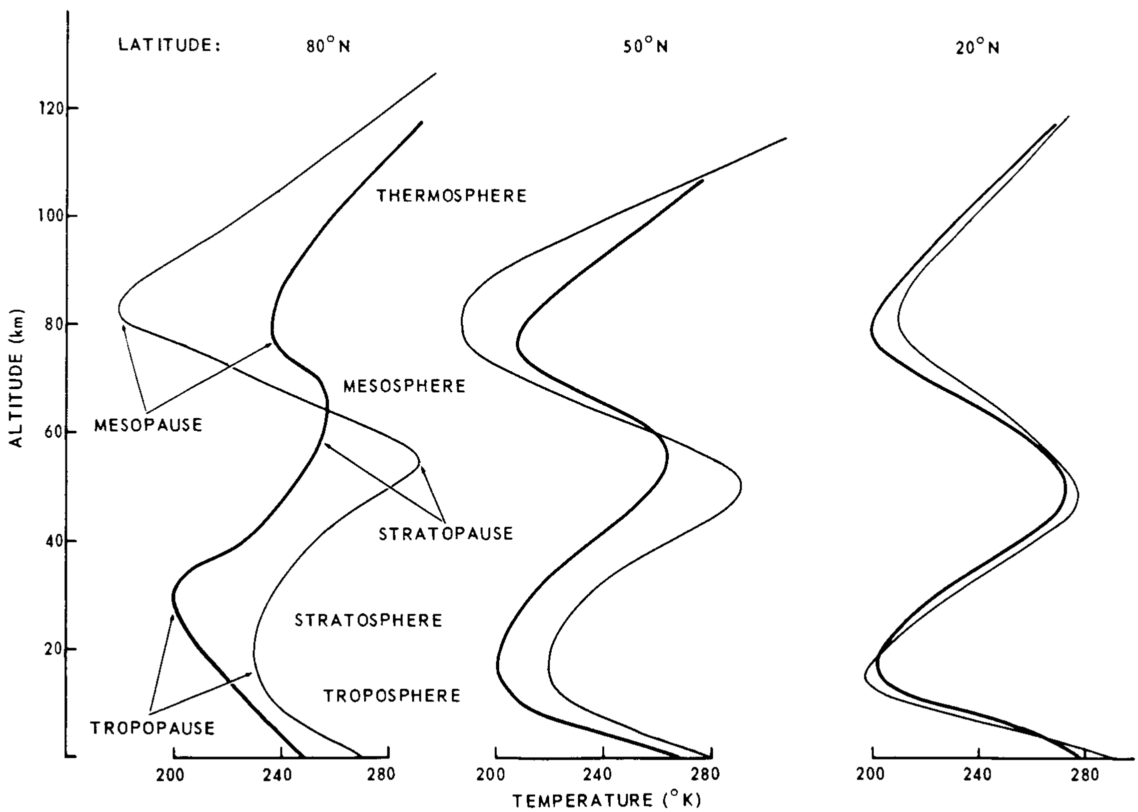

Figure 13 - Vertical distributions of atmospheric temperature at three different geographic latitudes. Light and heavy lines correspond to the summer and winter seasons respectively.

Table 4
Heights and Temperatures of Characteristic Levels in the Polar Regions

Level	Height (km)	Temperature (°K)
Tropopause—Summer	6 - 12	230 - 240
Winter	30 - 35	200 - 210
Stratopause—Summer	50 - 55	280 - 290
Winter	60 - 70	250 - 260
Mesopause —Summer	80 - 85	170 - 180
Winter	75 - 80	230 - 250
Thermopause	~550	1000 - 1500*

*The temperatures above mesopause might change widely with solar activity rather than with seasons (Reference 44).

The atmospheric temperature up to the 35 km level can be measured directly by balloon borne thermographs. The temperature levels above 35 km are observed by rockets, and those above 150 km by satellites (Table 5). It should be noted that temperatures above balloon altitudes are deduced from the air densities or pressures observed by the rocket borne instruments or by satellite drag variations. Since the densities deduced from satellite drag variations correspond to those at perigee, and since the atmospheric measurements made by rockets above 100 km are not sufficient to show latitude dependence, the variation of atmospheric structure with latitude above the mesopause still is not clear. Therefore, the atmospheric model based on the Rocket Panel Data

Table 5
Methods of Obtaining Atmospheric Temperature Observations

Method of Measurement	Altitude Range (km)	Observed Quantity
Balloon Borne Thermograph	0 - 35	Temperature
Rocket Borne Pressure Gages	30 - 100	Pressure, Density
Grenades Ejected from Rockets	30 - 90	Temperature
Rocket Borne UV Spectrograph	20 - 70	Temperature
Falling Spheres from Rockets	15 - 90	Density
Searchlight Beams	10 - 70	Density
Satellite Drag	~160	Density
Zenith Scattered Twilight	30 - 150	Density
Meteors (Photographic)	50 - 120	Density

(Reference 28) and on Kallmann's Table (Reference 29), can be acceptable for density distribution considerations even for the polar regions (Figure 14, the corresponding curves for atmospheric depth as a function of altitude were shown in Figure 4).

Recently, large diurnal variations of air density have been found above 200 km from analyses of satellite drag (References 13 and 46). The amplitudes are less than 2 percent at 200 km, but are more than 100 percent at 660 km. The amplitude increases with height, reaching a sharp maximum at 2 p.m. local time and gradually decreasing to a minimum at 6 a.m. However, this variation is negligible below 200 km and is dependent upon solar activity. In estimating the dissociation rate of molecular oxygen, these diurnal and latitudinal variations of upper air density may be neglected, since their contributions above 200 km are negligible.

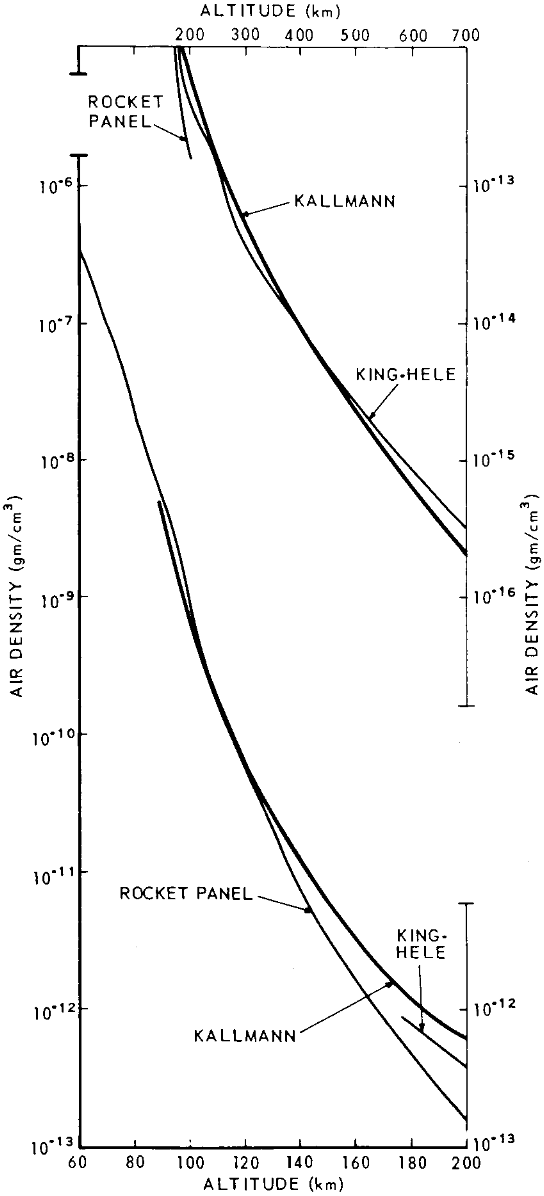

Figure 14 - Air density $\rho(z)$ versus altitude z. The atmospheric model used in the present calculation is based upon the following data: $z \leq 110$ km, Rocket Panel (Reference 28); $400 \geq z > 110$ km, Kallmann and Juncosa (Reference 45); and $z > 400$ km, King-Hele (Reference 30).

Vertical Distribution of Atmospheric Constituents

Rocket measurements have revealed that the main atmospheric composition remains the same from ground level to the mesopause, except for the decreasing concentrations of water vapor with altitude, and for the fractional presence of ozone in the lower stratosphere and upper troposphere (Reference 47). Above the mesopause, at an altitude of around 85 km, the composition of the atmosphere changes with altitude because of the partial dissociation of oxygen and the vertical diffusion of air. In the upper atmosphere, there is no technique available at present for measuring atomic oxygen concentration, but the total amount of molecular oxygen above a certain level has been measured as a function of altitude between 100 and 180 km (References 48 and 49). By the use of these data, the proportion of molecular oxygen in the overhead atmosphere is found to decrease above the mesopause, indicating that the oxygen is increasingly dissociated with altitude. However, because of the diffusive transport of molecular and atomic oxygen, the deficiency of molecular oxygen with altitude does not provide a basis for determining the degree of dissociation of molecular oxygen at each level (Reference 50). The vertical distributions of atomic and molecular oxygen above the stratosphere have been estimated theoretically by Chapman (Reference 51), Rakshit (Reference 52), Penndorf (Reference 53), and recently by Nicolet (References 54 and 42). These estimations are all based upon the photo-dissociation of oxygen molecules by solar radiation. Johnson's estimation (Reference 44) of the relative concentration by volume of the main atmospheric constituents is shown in Figure 15. The corresponding relative concentration by weight is presented in Figure 16.

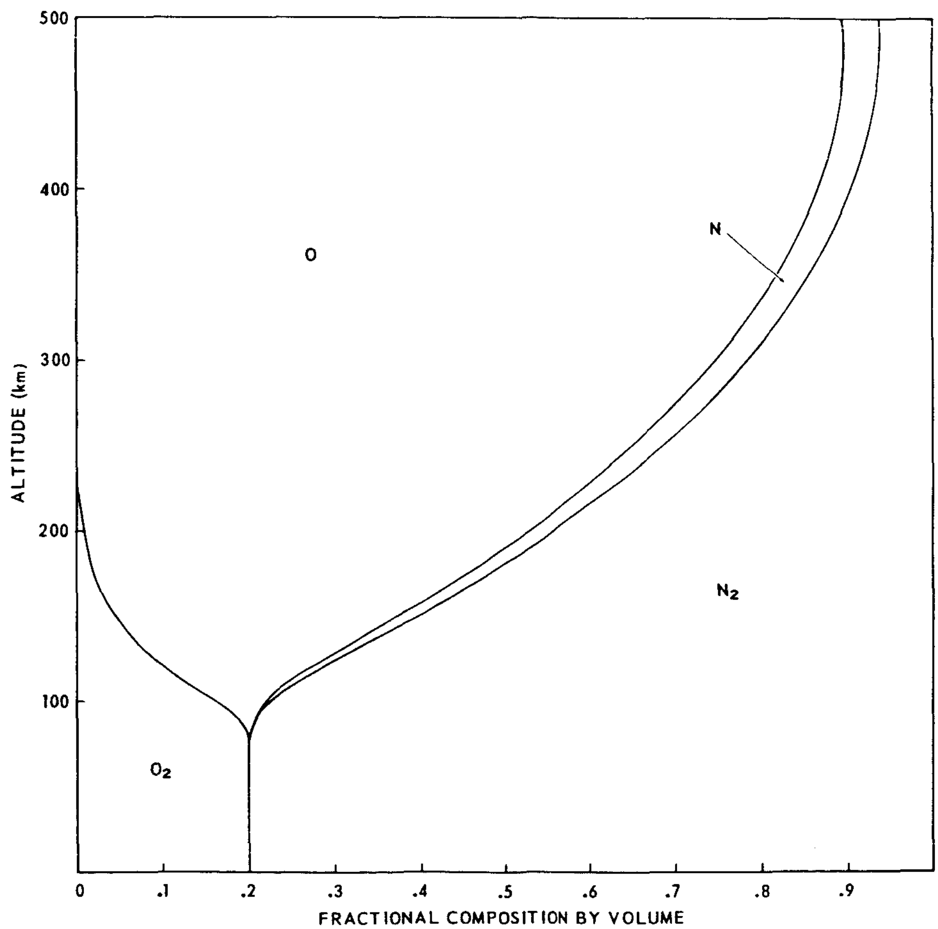

Figure 15 - Fractional composition of air by volume as a function of altitude

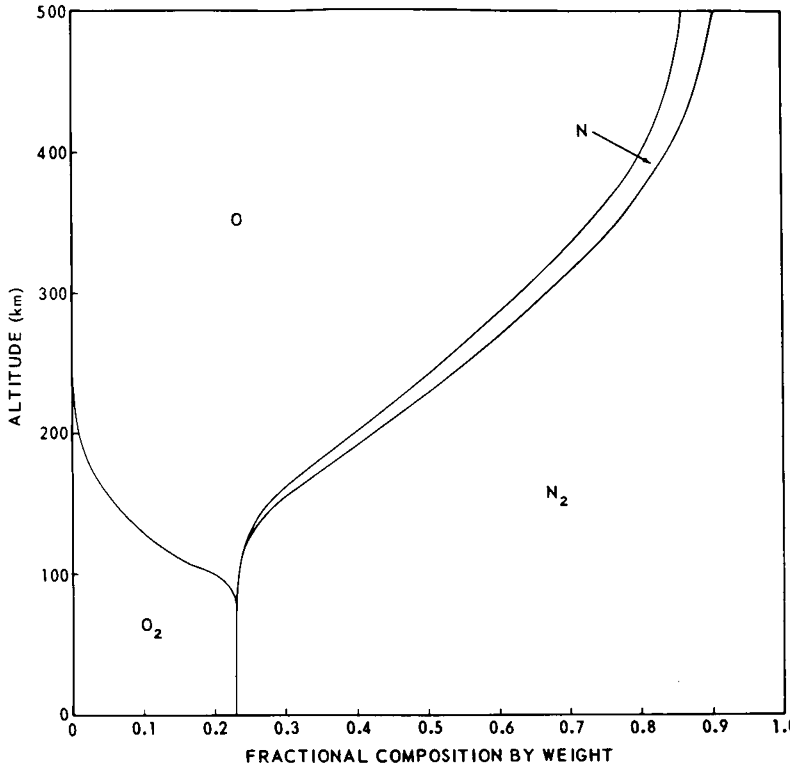

Figure 16 - Fractional composition of air by weight as a function of altitude

HEATING OF THE POLAR UPPER ATMOSPHERE

Rate of Dissociation of Molecular Oxygen by the Auroral Particles

According to the Frank-Condon Principle, oxygen molecules will dissociate upon the impact of charged particles or photons with kinetic energies higher than 5.08 ev. This value corresponds to the transition energy threshold from the ground level ${}^3\Sigma_g^-$ to the lowest repulsive level ${}^3\Sigma_u^-$.

The total cross section of the dissociation of molecular oxygen by electrons was measured by Glocker and Wilson (Reference 55), and estimated theoretically by Massey (Reference 56) and Mott (Reference 57). By combining these results, the total cross section of the dissociation of the oxygen molecule by electrons is obtained as a function of the energy of impact electrons. The total cross section of O_2 dissociation by electrons increases sharply around 5 ev, reaches a maximum at 8 ev, and declines at about 30 ev as the inverse of E (Figure 17). The maximum value of this cross section is on

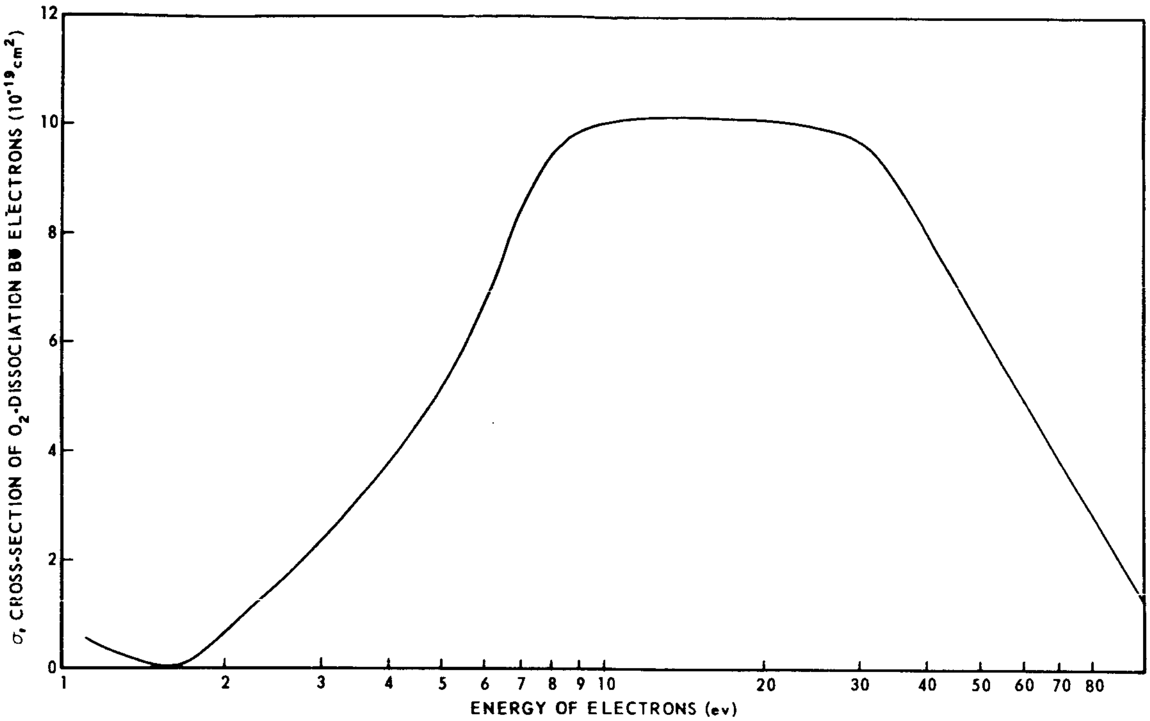

Figure 17 - Total cross section of O_2 dissociation by electrons as a function of kinetic energy of impact electrons

the order of 10^{-18} cm^2, which is of the same order as the molecular cross section estimated from the absorption coefficient of the Schumann-Range band (1751 - 1400A; 6.7 - 9.7 ev)—one of the most effective bands for the photo-dissociation of oxygen molecules. It is interesting to note that the efficiencies of O_2 dissociation, by electrons and photons around the energy levels of 10 ev, are both of the same order.

On the other hand, the dissociation of molecular oxygen by the direct impact of protons is not important, since the effective energy for dissociation is below 30 ev. Thus, the effective particles for O_2 dissociation are not composed of primary particles but mainly of secondary and tertiary particles produced in the air by the incoming primary protons and electrons.

In this respect the total specific ionization $j_t(E)$ is a most convenient quantity, since it is the total number of ion-pairs per gm/cm^2 produced by primary particles of energy E (in ev) and by all secondary electrons (Reference 24, p. 45). The total specific ionization is

$$j_t(E) = \frac{1}{V_o} k(E) , \tag{18}$$

where $k(E)$ corresponds to the primary ionization given by $-dE/dx$ (or $-dE/dR$) in Equation 1. V_o, the average energy expended per ion pair produced, is determined experimentally:

$$V_o = \begin{cases} 32 \text{ ev for electrons in air} \\ 36 \text{ ev for protons in air.} \end{cases}$$

Since the energy distribution of electrons ejected in the process of primary ionization is fairly uniform (Reference 57), the number of secondary electrons increases with an increase of primary energy (as given by Equation 18). This relationship can also be explained by the following: The energy of the primary particle in the air is spent in exciting and ionizing the air molecules. The secondary electrons thus produced will continue to lose energy by inelastic collisions as long as their energies are greater than the lowest excitation potential of the atoms in the air. A highly excited atom may lose energy by emitting a photon or an Anger electron. The degradation of the initial energy continues until only a certain number of atoms in the lowest ionized level, and a certain number of electrons and photons of a few ev energy, remain (Reference 24).

Atmospheric oxygen above 80 km is dissociated by solar radiation (photo-dissociation) in the following spectral bands (see Figures 15 and 16):

(1) Schumann-Runge continuum, 1400 - 1751A, ($\sigma \approx 10^{-19}$ cm^2);

(2) Herzberg continuum, 2200 - 2424A, ($\sigma \approx 10^{-24}$ cm^2); and

(3) Chappius band 4400 - 7400A, ($\sigma \approx 10^{-21}$ cm^2).

The Chappius band in the visible region is effective only for the dissociation of atmospheric ozone, which exists mostly in lower stratosphere. Consequently, the contribution of this band can be neglected in this problem. The σ's in parentheses, obtained from absorption measurements, are the total cross sections for O_2 and O_3 dissociation.

The degree of O_2 dissociation is determined by the equilibrium between the rate of dissociation due to solar radiation and the rate of association due to two body and three body collisions. The details of the photo-dissociation of atmospheric oxygen are given by Mitra (Reference 1) and by Nicolet (References 42 and 54).

Since the sun is very close to the horizon during the winter in the polar region, the effect of photo-dissociation is very weak or negligible. The lifetime of atomic oxygen in the mesosphere after sunset is presented, according to Nicolet (Reference 54), in Table 6.

Table 6
The Lifetime of Atomic Oxygen in the Mesosphere After Sunset

Height (km)	Lifetime (sec)
80	$9.4 \times 10^5 \approx$ 10 days
90	$3.3 \times 10^6 \approx$ 1 month
100	$9.8 \times 10^6 \approx$ 4 months

Since the existence of atomic oxygen in the polar mesosphere is not negligible even in the winter, two extreme cases of O_2 distributions will be considered. One case is maximum dissociation, in which most of the oxygen above the 80 km level is dissociated by vertically incident insolation as shown in Figures 15 and 16. The other case is that of no dissociation, in which the vertical distribution of molecular oxygen is simply given by the air density distribution (Figure 14), multiplied by the constant relative concentration, 0.23.

The rate of O_2 dissociation $r_p(z)\ dz$ at the altitude z by auroral protons is

$$r_p(z)\ dz = \int_{E_m}^{\infty} N(z) \left[\int_{W_o}^{E} \sigma(W)\ j_{t,p}(W,E,z)\ dW \right] i_p(E,z)\ dE\, dz\ , \tag{19}$$

where

$N(z)$ is the number density (cm^{-3}) of molecular oxygen;

$\sigma(W)$ is the differential cross section (cm^2) of O_2 dissociation by electrons of energy W;

$j_{t,p}(W,E,z)$ is the number $(gm/cm^2)^{-1}$ of secondary electrons of energy W, produced by protons of energy E per unit thickness of air at the altitude z;

$i_p(E,z)$ is the omnidirectional differential-intensity of auroral protons at the altitude z (in km), which corresponds to the atmospheric depth x (in gm/cm^2). (This is given by Equation 11 and shown in Figure 5);* and

W_o and E_m are, respectively, the threshold energy for O_2 dissociation and the lowest energy.

The number density of molecular oxygen is

$$N(z) = N_L \frac{\rho_a(z)}{\rho_{a,o}} C(z) = 2.16 \times 10^{22}\ \rho_a(z)\ C(z) \tag{20}$$

where

N_L is the Loschmidt number, $2.687 \times 10^{19} \approx 2.7 \times 10^{19}\ cm^{-3}$;

$C(z)$ is the fractional composition of O_2 by weight as shown in Figure 16;

---

*Equation 11 shows the omnidirectional differential range spectrum of spiraling protons at the depth x, $i_x(R)$, which is easily transformed into $i_z(E)$ by

$$i_z(E) = i_z(R)\ \frac{dR}{dE} = i_x(R)\ \frac{dR}{dE}.$$

The x-z curve is given in Figure 4 for protons and $\frac{dR}{dE}$ is shown in Figure 1.

$\rho_a(z)$ is the air density at the altitude z, in g cm^{-3}; and

$\rho_{a,o}$ is the air density at N. T. P., $1.2929 \times 10^{-3} \approx 1.3 \times 10^{-3}$, in gm/cm^3.

In the integrand of Equation 19, the terms inside the brackets can be written as:

$$\int_{W_o}^{E} \sigma(W)\ j_{t,p}(W,E,z)\ dW \approx \frac{\sigma_{int}}{W_e} \frac{k_p(E)}{V_{e,p}} \rho(z) ,$$

where

$\sigma_{int} = \int_{W_o}^{\infty} \sigma(W)\ dW \approx 6 \times 10^{-17}\ cm^2\ ev$ is the integral cross section of O_2 dissociation by electrons (see Figure 17);

W_e is the effective energy for O_2 dissociation, about 20 ev;

$\frac{k_p(E)}{V_{o,p}}$ is the total specific ionization of a proton with energy E in the air (i.e., the number of secondary electrons per unit depth of air in $(gm/cm^2)^{-1}$), where $V_{o,p} = 36$ ev; and

$\rho(z)$ is the air density at the altitude z, (gm/cm^3), $\rho(z) = \rho_a(z)$.

Evaluating the foregoing equation, we have

$$\int_{W_o}^{E} \sigma(W)\ j_{t,p}(W,E,z)\ dW \approx 8.33 \times 10^{-20}\ \rho_a(z)\ k_p(E) . \tag{21}$$

Substituting Equations 20 and 21 into Equation 19, we finally obtain

$$r_p(z)\ dz \approx 1.8 \times 10^3\ \rho_a^2(z)\ C(z) \int_{E_m}^{\infty} k_p(E)\ i_p(E,z)\ dE\ dz , \tag{22}$$

where $k_p(E)$ is shown in Figure 1. Similarly, the rate of O_2 dissociation due to auroral electrons at the level z is given by

$$r_e(z)\ dz \approx 2.0 \times 10^3\ \rho_a^2(z)\ C(z) \int_{E_m}^{\infty} k_e(E)\ i_e(E,z)\ dE\ dz ,$$

where $k_e(E)$ is shown in Figure 7.

The omnidirectional differential intensity of electrons, $i_e(E,z)$, is shown in Figure 11 for the case of the incident energy spectrum, $aE^{-4}\,dE$. It should be noted that the square of atmospheric density in Equations 22 and 23 is due primarily to the target distribution (the O_2 density in the atmosphere given by Equation 20) and secondarily to the reduction of the rate of ionization loss of primary particles from ev per gm/cm^2 to ev per cm.

The values $r_p(z)$ and $r_e(d)$, normalized to the incident total intensity, are shown in Figure 18 and Figure 19 respectively. (Incident total intensities are 3 x 10^6/cm^2-sec with the differential spectrum $E^{-2.8}dE$ for protons, and 5.2 x 10^6/cm^2-sec with $E^{-4}dE$ for electrons, respectively.)

For these numerical calculations the two extreme cases of $C(z)$ are assumed: the minimum distribution of O_2 (O_2 is photo-dissociated by vertical insolation); and the maximum distribution of O_2 (non-photo-dissociation) in the atmosphere. The effect of photo-dissociation on the dissociations by auroral particles clearly is negligible below the mesopause (about 85 km), where the dissociation by auroral particles is most effective.

In order to calculate the final atomic oxygen distribution due to O_2 dissociation by auroral particles, we must assume the duration of the aurora, the total flux of incident particles (or total energy flux), and the rate of association at different altitudes. Instead of presenting cases with several combinations of these factors, the following points are made:

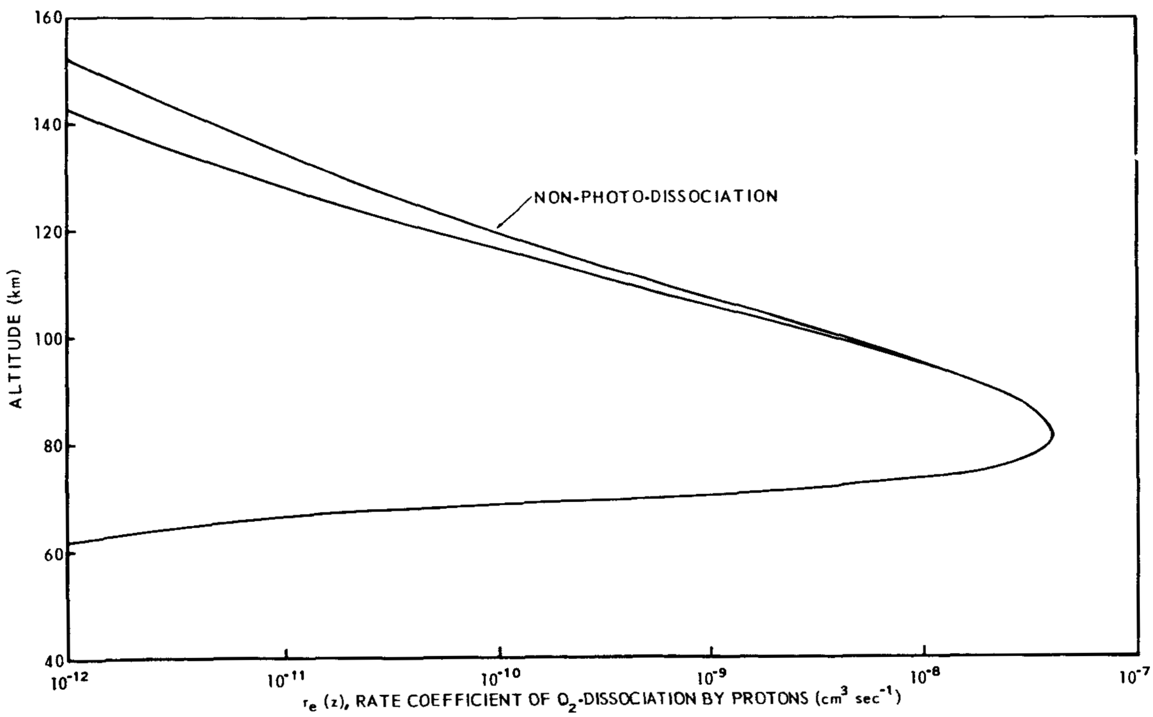

Figure 18 - Rate coefficient for O_2 dissociation by auroral protons with differential spectrum $E^{-2.8}dE$, as a function of altitude

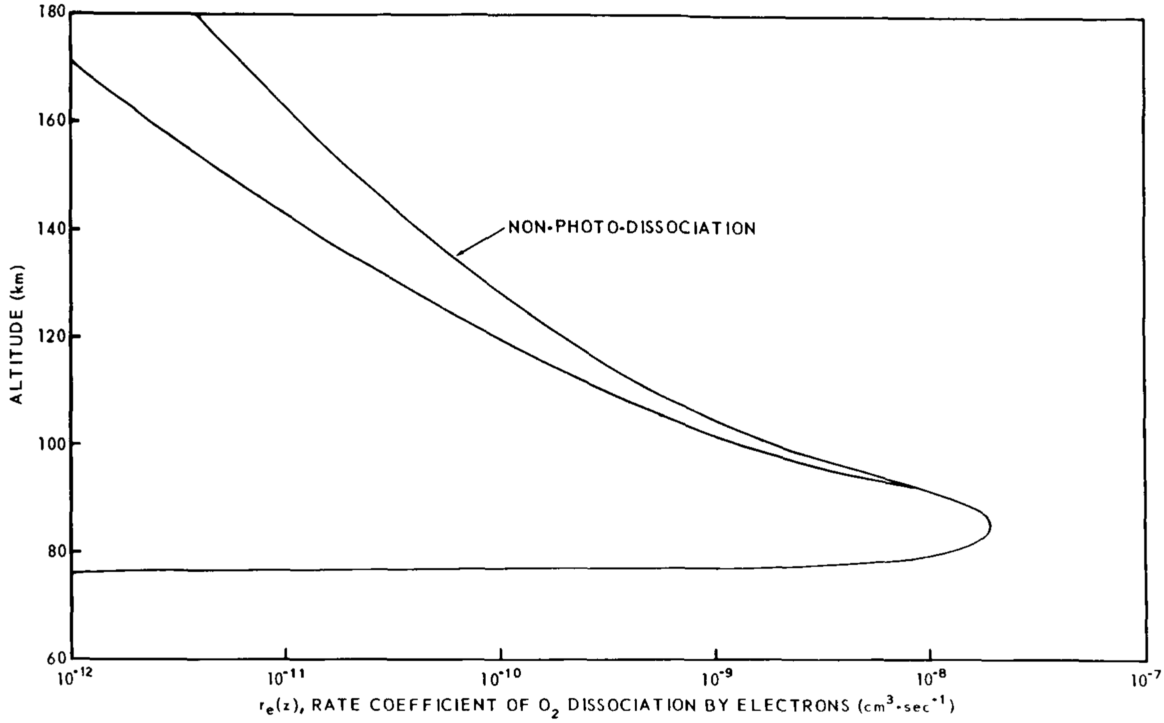

Figure 19 - Rate coefficients for O_2 dissociation by auroral electrons with differential spectrum $E^{-4}dE$, as a function of altitude

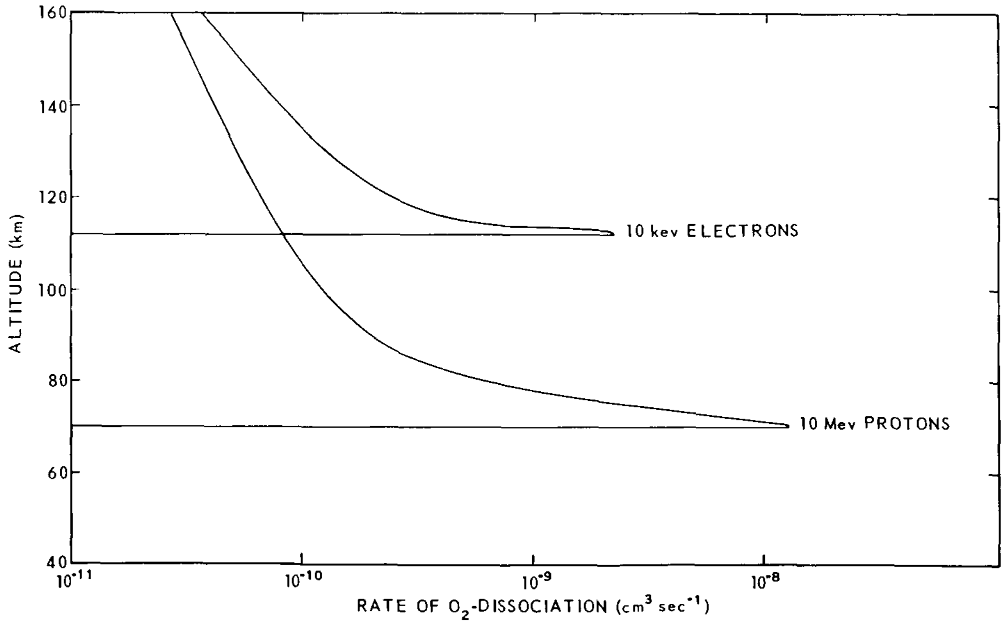

Figure 20 - Rates of O_2 dissociation by monoenergetic electrons and protons in the upper atmosphere, normalized for initial total intensity (rate coefficients) as functions of altitude

1. The rate coefficient of O_2 dissociation due to auroral particles is almost the same as that due to the insolation (solar ultraviolet).

2. The profile of the atomic oxygen production rate in the atmosphere due to auroral particles depends on the energy spectrum. If the incident particles are mono-energetic, the lower boundary of the profile becomes very steep, as is shown in Figure 20 where the case for 10 kev electrons and the case for 10 Mev protons are plotted. These lower boundaries, given in terms of the penetration depth of spiraling particles, are drawn in Figure 21 by using the atmospheric depth-altitude relation and the energy-range relation curves for protons in the air.

If the flux of auroral electrons is of the order of $10^{12}/cm^2$-sec, as has been observed by rocket penetration into the active aurora (Reference 25), the rate of O_2 production due to electrons will be of the order of 10^4 atoms/cm^3-sec at the level of maximum production (about 85 km). This figure can be regarded (Reference 54) as comparable with the rate coefficient for photo-dissociation caused by solar radiation (the Schumann-Runge continuum), which is the order of 10^5 atoms/cm^3-sec at the production peak (around 90 km). Therefore it can be expected that, during severe aurorae, a large fraction of molecular oxygen molecules are dissociated by auroral particles, and the rate of dissociation is comparable with that due to solar ultraviolet.

Since the rate of association of atomic oxygen is smaller at higher altitudes, the maximum concentration of atomic oxygen should be at a higher altitude than the production peak of atomic oxygen, and will be near 110 km in the case of photo-dissociation. According to Nicolet's estimation, the maximum concentration of oxygen atoms under the equilibrium condition for the dissociation rate of 10^4 atoms/cm^3-sec is the order of 10^{11} atoms/cm^3 at the 110 km level.

It has been shown that, if there is no strong downward advection above the mesosphere, the lifetime of atomic oxygen around the altitude of maximum concentration (> 100 km) is more than 4 months, but at the altitude of the production peak (about 85 km), it is less than one month. However, if there is a strong subsidence in polar region in late winter, these lifetimes

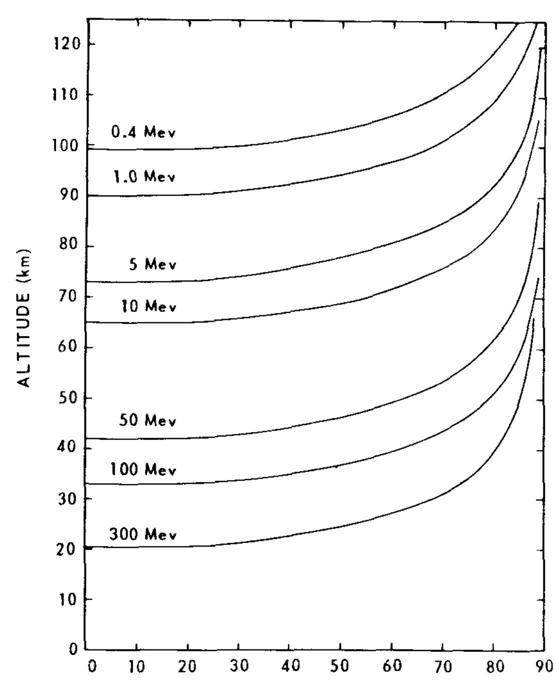

Figure 21 - Penetration depth of spiraling mono-energetic protons in the atmosphere as a function of the pitch angle α

of oxygen atoms should be shortened drastically. In this respect, the production of oxygen atoms by auroral particles in the polar upper atmosphere during late winter (from January to March) might play an important role in supplying the atomic oxygen that contributes to upper atmospheric heating during the polar night.

Energy Release from the Association of Oxygen Atoms

In a reverse process of endothermic dissociation of molecular oxygen (discussed in the foregoing section) the same amount of energy (5.08 ev per O_2 molecule) is released by the association of atomic oxygen.

The association of oxygen atoms into a molecule proceeds according to one of the following types of reactions:

(1) Radiative association:

$$O + O \rightarrow O_2 + h\gamma .$$

This reaction's rate coefficient, the radiative association coefficient, is $\alpha_R \approx 4 \times 10^{-21}$ cm^3/sec (Reference 58).

(2) Three body collision:

$$O + O + x \rightarrow O_2 + x' .$$

Here, the third colliding particle x' is not necessarily a neutral atom or molecule; even an electron can remove the excess energy after oxygen molecule formations. The coefficients of this reaction (non-radiative association) are known experimentally (References 1 and 58):

$$\begin{aligned} \alpha_n &= 5 \times 10^{-34} \sqrt{T}\, N_a \text{ cm}^3/\text{sec (if } x' \text{ is an atom or molecule)}, \\ \alpha_e &= 9 \times 10^{-35} \sqrt{T}\, N_e \text{ cm}^3/\text{sec (if } x' \text{ is an electron)}, \end{aligned} \tag{24}$$

where N_a and N_e are the number densities of air particles and electrons, respectively.

In general, the rate of association is expressed by

$$\frac{\partial N_o(z)}{\partial t} = \alpha \left[N_o(z)\right]^2 , \tag{25}$$

where the coefficient α is α_R, α_n, or α_e, corresponding to the reactions mentioned above. As can be seen, the radiative association is approximately proportional to the square of atmospheric pressure, while non-radiative association by collision is approximately proportional to the cube of the value of atmospheric pressure. Thus, the radiative association predominates only at the extreme altitudes above 300 km, and can be neglected in the present problem of upper atmosphere warming (Reference 59).

Furthermore, the number density of electrons, N_e, is actually very small as compared with the number density of air particles, N_a, even in the ionosphere, as is shown below:

D-region (60 ~ 80 km): $N_e < 10^4/cm^3$, $N_a \sim 10^{14}/cm^3$;

E-region (100 ~ 130 km): $N_e \sim 10^5/cm^3$, $N_a \sim 10^{13}\ cm^3$;

F-region (200 ~ 350 km): $N_e \sim 10^5/cm^3$, $N_a \sim 10^9\ cm^3$.

Therefore, the contribution of electrons to oxygen association by three body collisions is negligible; for this discussion, Equation 25 can be expressed as:

$$\frac{\partial N_o(z)}{\partial t} = \alpha_n \left[N_o(z)\right]^2 , \tag{26}$$

where α_n is given by Equation 24.

Obviously, the rate of oxygen molecule formation in the atmosphere is a function of the vertical distribution of atomic oxygen. Since, thus far, no direct measurements of atomic oxygen distribution in the upper atmosphere have been made, the present calculation will be performed by using the theoretical values, i.e., maximum distribution limited by the equilibrium between dissociation and association of atmospheric oxygen.

The rate of energy release, $dq(z)/dt$ (in ev/cm^3-sec) from the association of atomic oxygen at the altitude z is:

$$\frac{dq(z)}{dt} = \frac{\epsilon_0}{2} \frac{dN_o(z)}{dt} , \tag{27}$$

where ϵ_0 is the dissociation energy of the oxygen molecule, 5.08 ev (8.13×10^{-19} joules or 1.95×10^{-19} calory) per molecule. The factor 2 in the denominator in the right hand side of Equation 27 is due to the requirement of two atoms for one association.

Provided that the heat capacity of air at constant pressure, $C_p(z)$, is known, the rate of atmospheric temperature change at the level z due to the exothermic association of oxygen atoms, $dT(z)/dz$, can be estimated by

$$\frac{dT(z)}{dt} = \frac{1}{C_p(z)\ \rho_a(z)} \frac{dq(z)}{dt} , \tag{28}$$

where $\rho_a(z)$ is the air density at the level z in gm/cm^3, and $dq(z)/dt$ is given by Equations 26 and 27. The local change of number density of atomic oxygen, $\partial N_o(z)/\partial t$, should be written from the equation of continuity:

$$\frac{\partial N_o(z)}{\partial t} = \frac{dN_o(z)}{dt} - \text{div}\left[\vec{v} \cdot N_o(z)\right], \tag{29}$$

where $\vec{v}$ is the velocity of the air flow (cm/sec). The warming rate of the upper air estimated by Equation 28 with Equations 26, 27, and 29 gives an overestimation unless the effect of cooling is taken into account.

RADIATIVE COOLING DUE TO $^3P_1(O)$-$^3P_2(O)$ TRANSITION

Each neutral oxygen atom has eight orbital electrons with the ground state configuration $(1s)^2\ (2s)^2\ (2p)^4$. The last four electrons in the incomplete L-shell (2p electrons) give rise to the terms ^3P, ^1D, and ^1S. Among these levels ^1D and ^1S are metastable and the transition between them is forbidden, but is known to occur in a very rarified gas such as the upper atmosphere and to give the well known green line in the airglow and aurora (5577A). The transitions $^1D_2$-$^3P_1$, $^1D_2$-$^3P_2$ are the red lines in the auroral spectra. In the triplet term P level, $^3P_2$ is the lowest energy; i.e., the ground state of neutral atomic oxygen. The lowest excited states, $^3P_1$ and $^3P_0$, are 0.020 ev and 0.028 ev above the ground level, respectively. These excitation energies are equivalent to the kinetic energy of gases at temperatures of 240°K and 330°K, respectively.

According to Pasternack (Reference 60) the transition probabilities for $^3P_0$-$^3P_1$ and $^3P_1$-$^3P_2$ are 1.7 x 10^{-5}/sec and 8.9 x 10^{-5}/sec, respectively. Furthermore, the statistical weight of the $^3P_0$ state is less than half that of the $^3P_1$ state. Therefore, the first transition is insignificant by comparison with the second, and will be neglected.*

The mechanism of radiative cooling is as follows: By a two body collision an oxygen atom in the ground state, $^3P_2$, is excited to one of the lowest excited states, $^3P_1$. In this collision, a part of the thermal energy of encounter (O_2, and O, N and N_2, etc.) is transferred into the excitation energy of 0.02 ev per oxygen atom, which is emitted as a far infrared electromagnetic wave ($\lambda \approx 6.2 \times 10^{-3}$ cm) when the atom returns to the ground state. Since the optical depth above the 100 km for this long wave is very small, most of the radiated energy from this de-excitation is dissipated into outer space.

The excitation to $^3P_1(O)$ by collision is faster than emission in the upper atmosphere above 100 km level (Reference 59); therefore, the distribution of oxygen atoms between the excited states and the ground state is given by the thermodynamic equilibrium. According to Bates, the rate of de-excitation, $^3P_1(O)$-$^3P_2(O)$ at the level z, is

$$R(z) = B\ N_o(z)\ A(z)\ (\text{ev/cm}^3\text{-sec}), \tag{30}$$

*The contribution of other transitions of atomic oxygen, such as ^1D-^3P, to atmospheric cooling has been investigated by Spitzer (Reference 61) and others, but it has been shown that these are also insignificant when compared with that of $^3P_1$-$^3P_2$ (Reference 59).

where B is the constant 5.8 x 10^{-7}; $N_o(z)$ is the number density of atomic oxygen in ^3P states per cm^3. The factor $A(z) = A[T(z)]$, resulting from the statistical distribution of the states in thermodynamic equilibrium, is given by

$$A(z) = \frac{3\omega_1 \exp\left(-\frac{\epsilon_1}{kT(z)}\right)}{\omega_2 + \omega_1 \exp\left(-\frac{\epsilon_1}{kT(z)}\right) + \omega_o \exp\left(-\frac{\epsilon_0}{kT(z)}\right)},$$

where ω_o, ω_1, and ω_2 are the statistical weights of the levels $^3P_0$, $^3P_1$ and $^3P_2$, and are numerically equal to 1, 3, and 5 respectively; and ϵ_1 and ϵ_o are the excitation energies 0.020 ev and 0.028 ev, respectively. The coefficient $A(z) = A[T(z)]$ is approximately unity for atmospheric temperatures above the mesosphere; and

$$A(z) \approx \begin{cases} 1 & \text{for } T(z) \approx \infty°K \\ 0 & \text{for } T(z) \approx 0°K . \end{cases}$$

The optical depth for far infrared ($^3P_1$-$^3P_2$) emission is less than 0.3 above 100 km. Therefore, the corresponding reducing factors, which are to be multiplied to the right hand side of Equation 30, can be regarded as unity. The rates of energy loss of air are shown in Figure 22 by dashed curves, assuming the temperature $T(z)$ as a parameter.

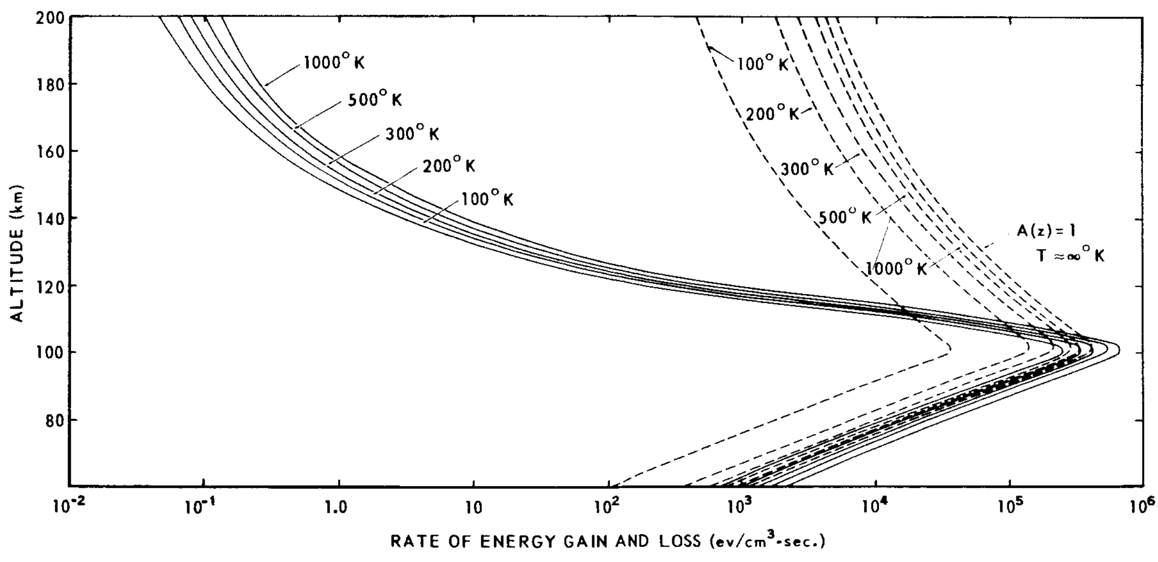

Figure 22 - Rates of energy gain owing to oxygen association (solid curves), and of energy loss owing to $^3P_1(O)$-$^3P_2(O)$ transition (dashed curves) as functions of altitude, for different atmospheric temperatures $T(z)$

The number density of atomic oxygen, $N_o(z)$, and of air, $N_a(z)$, are shown in Figure 23 for altitudes between 60 and 200 km;* another distribution curve of atomic oxygen (Reference 52) is presented for comparison.

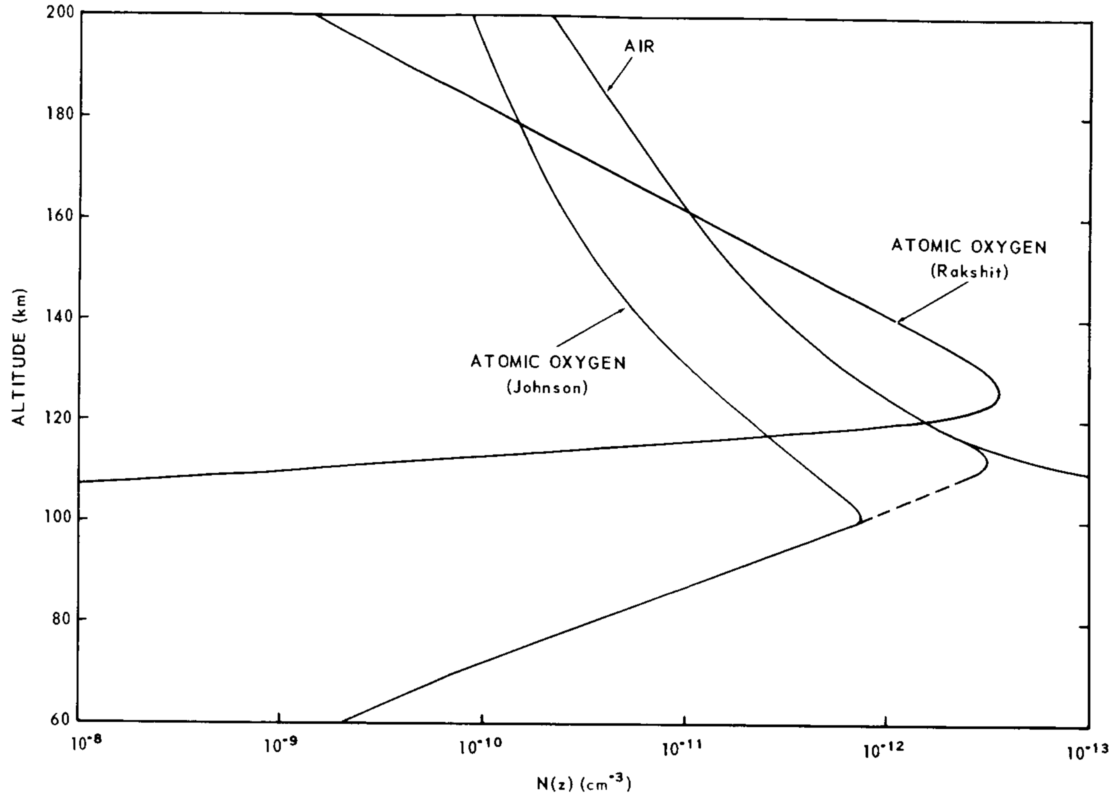

Figure 23 - Number density of air particles, $N_a(z)$ and of atomic oxygen, $N_o(z)$, as functions of altitude z

Heating by the Association of Atomic Oxygen

The energy gains per cm^3 of air per second, given by Equation 26 with Equation 24, are shown in Figure 22 for different initial atmospheric temperatures. These curves

*In this figure, the number density of atomic oxygen is calculated as follows: Division of the mean molecular weight of air, $M_a(z)$, by Avogadro's number, 6.026×10^{23}, gives the average mass of the air molecules, $m_a(z)$; hence the number density of air at each level is

$$N_a(z) = \frac{\rho_a(z)}{m_a},$$

where $\rho_a(z)$ is the density of air. Therefore, the number density of atomic oxygen per cm^3 is

$$N_o(z) = c(z)\, N_a(z) \frac{m_a}{m_o},$$

where $c(z)$ is the fractional composition of atomic oxygen by weight and m_o is the mass of the oxygen atom.

are calculated with respect to the vertical distribution of oxygen atoms given by Johnson (see Figures 15 and 16). This estimation of atmospheric heating and cooling is, however, based on the static atmosphere, in which it is assumed that no vertical air flow and diffusion exist. In such an atmosphere, the equilibrium exists only at 110 km or below, depending on the vertical distribution of atomic oxygen.

In Figure 24, the net gains of thermal energy due to the aforementioned processes are plotted against altitude, assuming several values of atmospheric temperature $T(z)$. If vertical air flows and diffusions are neglected, the air below a certain level (around 110 km or lower depending on the distribution of atomic oxygen) is continuously warmed by association of atomic oxygen; and above that level the air is continuously cooled by the far infrared emission of atomic oxygen. The positions of maximum heating and maximum cooling are very close (within several kilometers of each other), and their proximity reduces the stability of the layer between them. Therefore, the contribution of diffusion or vertical air movement around these levels is very important for calculating equilibrium temperature distribution; i.e., it is meaningless to try to estimate the equilibrium temperature around these levels, ignoring the diffusion or the vertical movements of air. The diffusions of atomic and molecular oxygens in the upper atmosphere are estimated theoretically by Nicolet and Mange (Reference 58); but the results are very sensitive to the vertical distribution of oxygen atoms and molecules, and the coefficients of eddy diffusion around these heights are not well established. Therefore, in this paper, only the effect of vertical flow will be considered.

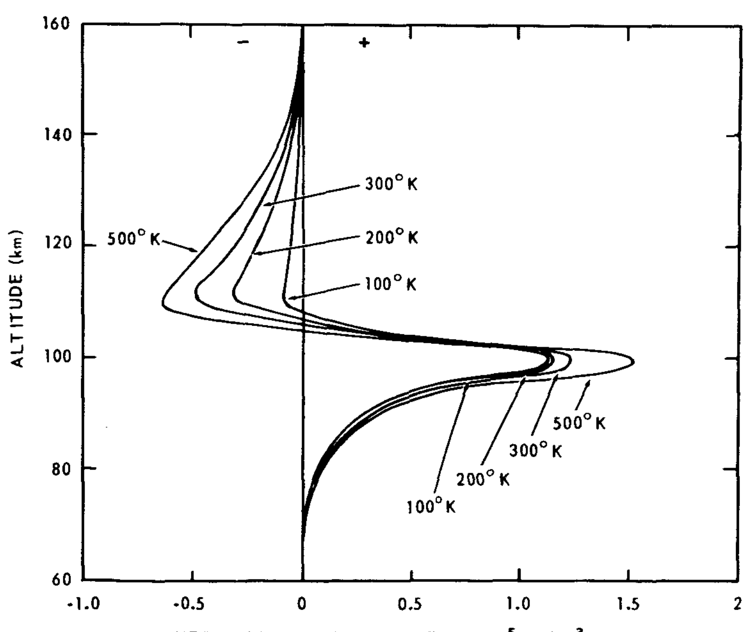

Figure 24 - Net gain of thermal energy as a function of altitude, for different atmospheric temperatures $T(z)$ as a result of the two processes shown in Figure 22

Effect of Subsidence on the Association of Oxygen

When a volume of dry air descends by external force, the temperature of the air increases with increasing pressure. This rate of increase is known as the adiabatic lapse rate of dry air:

$$\frac{dT(z)}{dz} = -\frac{g}{C_p} = -9.76 \times 10^{-5}\ ^{\circ}\mathrm{C/cm},$$

where g is acceleration of gravity, 980.67 cm/sec.^{2}

The constant C_p is specific heat of air at constant pressure and is equal to 0.24 cal/gm-°C in the homosphere; but C_p increases with altitude to approximately 0.3 cal/gm-°C at 300 km (Reference 15). Therefore, the rate of temperature change due to adiabatic compression, with vertical velocity v_z (in cm/sec), is

$$\frac{dT(z)}{dt} \approx -9.8 \times 10^{-5}\ v_z\ ^{\circ}\mathrm{C/sec.} \tag{31}$$

When one gram of air containing $c(z)$ grams of atomic oxygen descends, the temperature increases not only by adiabatic compression, but also by the increasing exothermic association of oxygen. By neglecting the horizontal divergence, the latter can be estimated by using Equation 29, which is written for the steady state of vertical air flows:

$$\begin{aligned} \frac{dN_o(z)}{dt} &= \mathrm{div}\ vN_o(z) \\ &\approx v_z \frac{\partial N_o(z)}{\partial z} \\ &\approx v_z \frac{\rho(z)}{m_o} \frac{\partial c(z)}{\partial z}. \end{aligned} \tag{32}$$

By noting Equation 27 and substituting Equation 32 into Equation 28, we get

$$\frac{dT(z)}{dt} \approx \frac{\frac{\epsilon_0}{2}}{C_p(z)\ m_o} v_z \frac{\partial c(z)}{\partial z} = 1.5 \times 10^{4}\ v_z \frac{\partial c(z)}{\partial z}\ ^{\circ}\mathrm{C/sec}, \tag{33}$$

where m_o, the mass of atomic oxygen, is 5.35×10^{-23} gm. This expression agrees with that derived by Kellogg (Reference 62).

The fractional content of oxygen atoms in air, $c(z)$—which is called by Kellogg (Reference 62) in an analogy to water vapor, the mixing ratio of atomic oxygen—and its gradient $dc(z)/dz$ are shown in Figure 25. The curves used by Kellogg (Reference 50) are also shown for a comparison. The vertical velocity needed to produce a heating of 10°C per day, estimated by Equation 33, is shown with Kellogg's results in Table 7. In the height of the minimum velocity, which corresponds to the maximum gradient of $c(z)$, and in the absolute values of descending velocity v_z, the differences between the present results and Kellogg's (last column), are due to the differences in the vertical distribution of oxygen atoms between Johnson's (Reference 6) and Nicolet's estimation (Reference 50).*

From Equation 31, a descending velocity of 1 km/day (more than 1 cm/sec) is necessary to warm the air at the rate of 10°C/day, by means of adiabatic compression. Comparing this figure with the values of v_z in Table 7, the warming by the exothermic association of atomic oxygen is seen to be more than one order more effective than the adiabatic warming due to subsidence of air. Moreover, the maximum warming due to oxygen

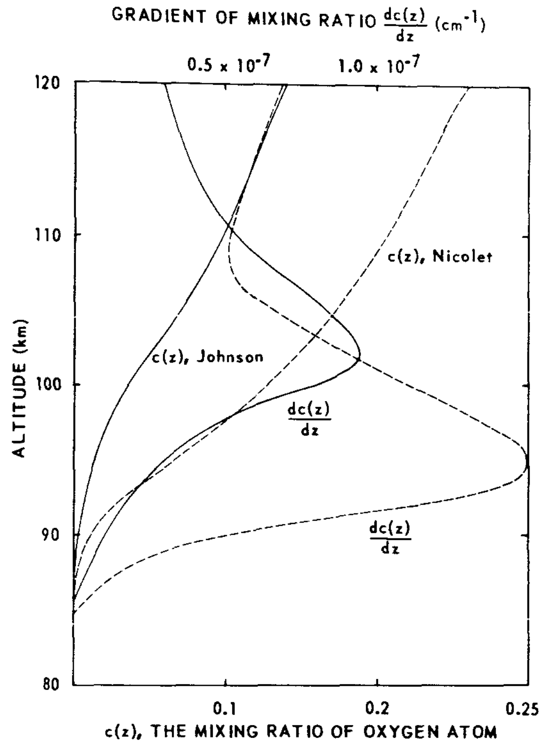

Figure 25 - Mixing ratio of atomic oxygen $c(z)$ and its vertical gradient $dc(z)/dz$ in the upper mesosphere. The dashed curves correspond to Nicolet's estimation, which were used by Kellogg in 1961.

Table 7
Descending Velocity Necessary for 10°C/day Warming

Height (km)	Mixing Ratio Gradient $\frac{dc}{dz}$ (cm^{-1})	v_z (cm/sec)	v_z (km/day)	v_z [Kellogg, 1960] (km/day)
80	~0	~∞	∞	∞
85	5×10^{-9}	1.4	~1.2	~0.6
90	10^{-8}	0.74	0.64	0.13
95	7.2×10^{-8}	0.10	0.09	0.04
100	8.0×10^{-8}	0.09	0.08	0.06
110	5.6×10^{-8}	0.13	0.11	0.13
120	4.6×10^{-8}	0.16	0.14	0.05

*The vertical distribution of atomic oxygen given by Rakshit (Reference 52) is omitted here, because it exceeds the total air density distribution curve at the 110 km level (Figure 23).

association is around the mesopause (between 90 and 100 km) for the uniform velocity of subsidence.

Although the subsidence in the upper polar atmosphere has not been measured directly, the convergent flow towards the pole above the 90 km level in winter has been indicated by several investigations (References 6 and 62-64). Therefore, as pointed out by Kellogg (References 6 and 62), the warm polar mesosphere must be maintained during the winter by the exothermic oxygen association intensified by the subsidence, which occurs in winter in polar regions as a part of the general circulations of the earth's atmosphere.

It should be noted that in the estimation of the cooling described above, only that due to the far infrared emission from oxygen atoms is considered; it is of the order of -3°C/day (Figure 24), and effective above 100 km or higher. Below this level, however, the cooling due to the infrared emissions from CO_2 (15μ), O_3 (9.7μ) and H_2O (50μ) become very important. According to Murgatroyd and Goody (Reference 65), the maximum cooling rate of air due to these infrared emissions appears around 65 km and is of the order of 10^{-4} watt/gm, corresponding to the cooling rate of -10°C/day in the vicinity of the mesopause.

ABRUPT WARMING OF THE POLAR UPPER AIR

The temperature variations observed at Thule, Greenland (geographic Lat. 76° 31'N, Long. 68° 50'W) of different isobar levels in the upper atmosphere during the period from January 26 to February 6, 1958, are shown in Figure 26. From this figure, the warming of air is seen to shift from the upper layers toward the attenuation increasing with atmospheric depth. The propagation of the warm layer is caused not by molecular or turbulent diffusion, nor by thermal conduction, but by the subsidence of air, since:

1. The propagation velocity is very large; within 24 hours, maximum temperature will shift from a 25 mb (~25 km) level to a 100 mb (~16 km) level. More than five days are required to shift the maximum temperature between these levels by the fastest thermal diffusion due to the turbulence.

2. There is an inversion in the temperature profile after the shifting of the maximum temperature to the lower layer.

Furthermore, this subsidence is indicated by rocket soundings at higher altitudes. The data of Figure 27 were obtained by rocket soundings made in conjunction with balloon observations during the winter of 1957-58 at Churchill, Canada (Reference 66). From these results, it is seen that the warm stratopause descends from 58 km to 45 km, increasing the temperature from 270°K to 290°K within four days. The largest temperature

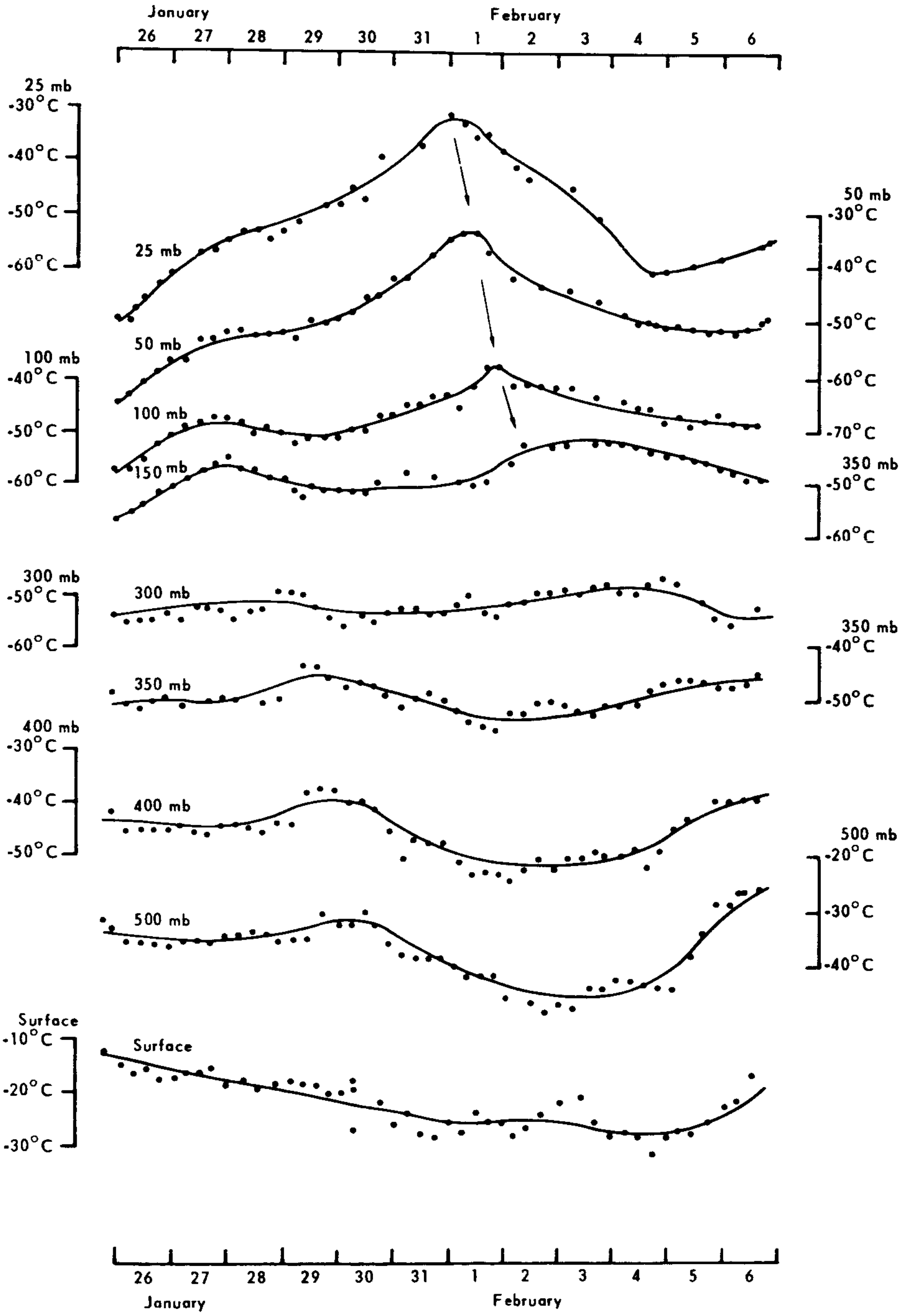

Figure 26 – Abrupt warming of the lower stratosphere observed a Thule (76.5°N), Greenland, in winter 1958

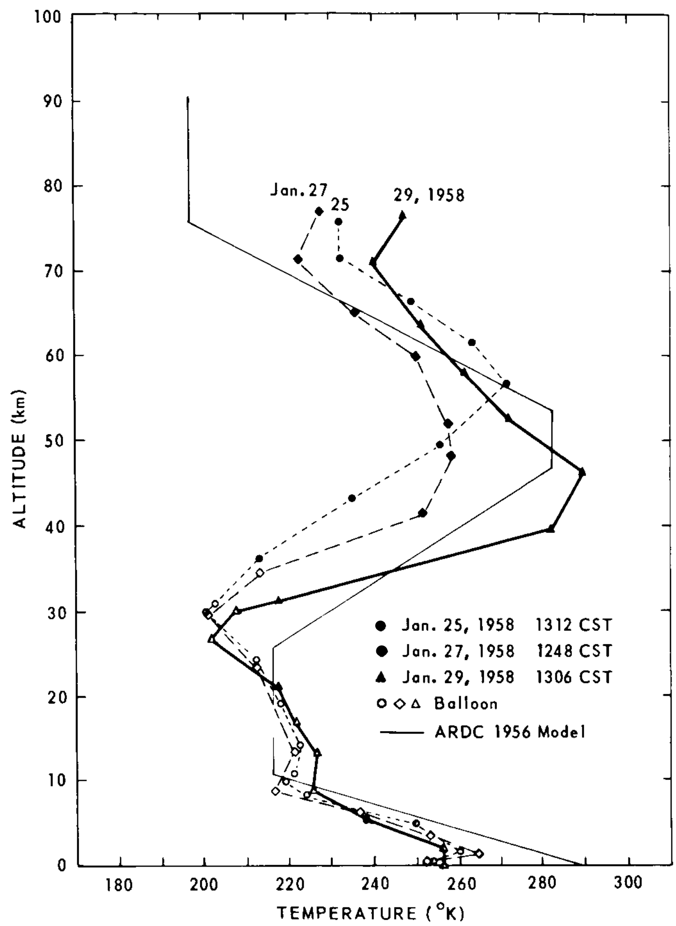

Figure 27 - Abrupt warming of the mesosphere and the upper stratosphere observed by rockets and balloons at Churchill (58.7°N), Canada, in the winter of 1957-58

increase observed at the 40 km level, almost 60°C, occurred during January 24-29. Although the abrupt warming shown in Figure 26 occurred in the dark shadow of polar night, this phenomenon is essentially the same as that first observed at Berlin in 1952 (Reference 67).

According to Scherhag (Reference 18) the center of warming first appeared in the 25 mb-chart near the eastern Mediterranean on January 21, 1958, and moved toward the northwest as shown in Figure 28. The maximum warming was observed around January 25 in the central part of Europe, around January 30 in Greenland (which corresponds to the results shown in Figure 26), and at the beginning of February in Northern Canada. It disappeared on February 8 off the Aleutian Islands. Figure 29 shows the rapid warming in the lower stratosphere observed simultaneously at four stations near the magnetic

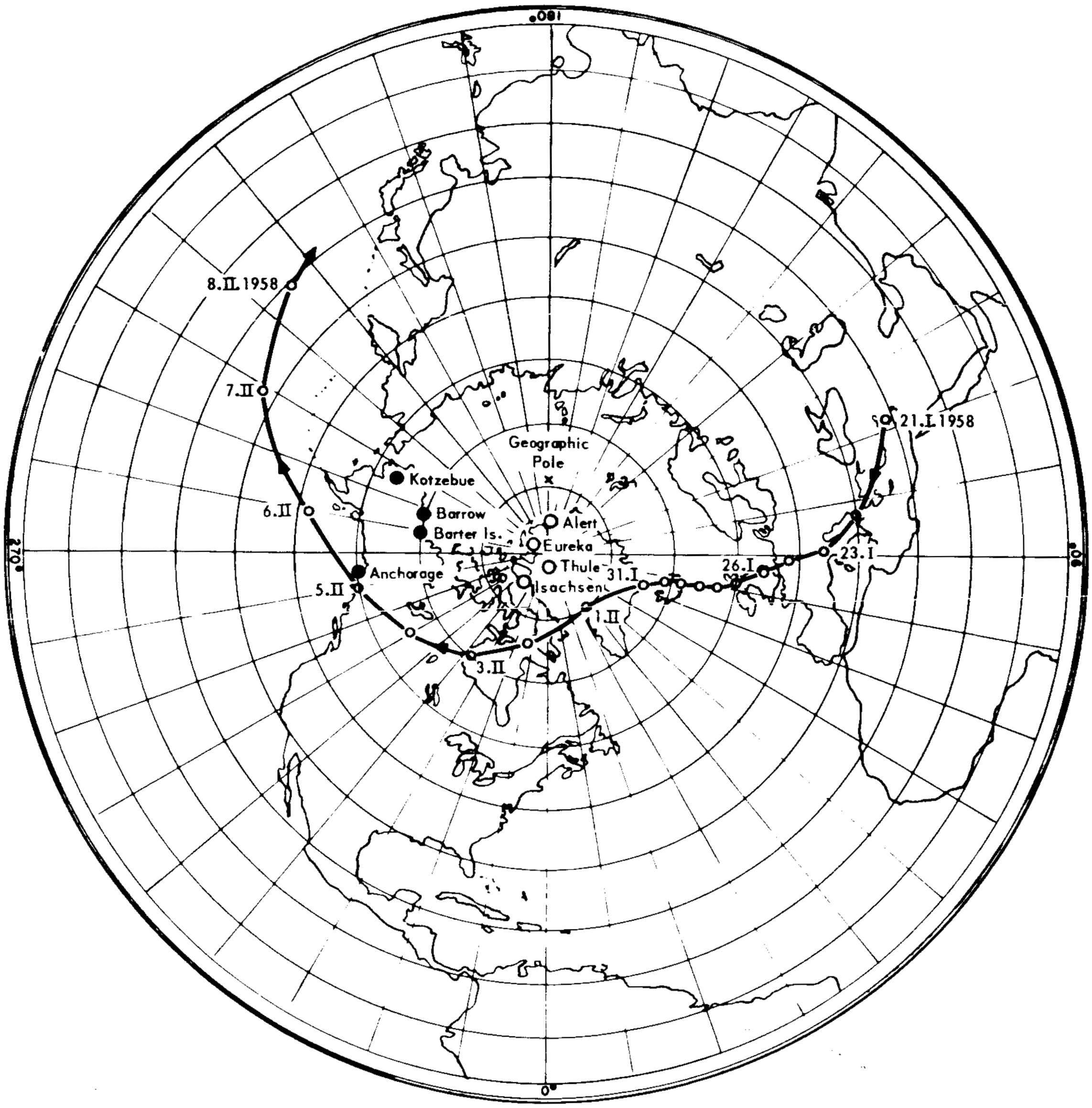

Figure 28 - Trajectory, in geomagnetic coordinates, of the warming center in the 25 mb-chart during the winter of 1957-58. Open circles show the locations of the stations where the abrupt warming of the stratosphere is observed simultaneously; closed circles, those where no warming is observed in the same period.

pole (Alert, Eureka, Isachsen and Thule). While no unusual warming was observed at other Arctic stations (Kotsebue, Barrow, Barter Island, and Anchorage, etc.) during the same period (Figure 30). Because of the lack of high altitude data, the foregoing results may not be conclusive. For example, according to Scherhag's analysis an increase of upper air temperature should be observed in Figure 30 around February 5 at Anchorage. However, these abrupt warmings are the result of large scale disturbances in the northern

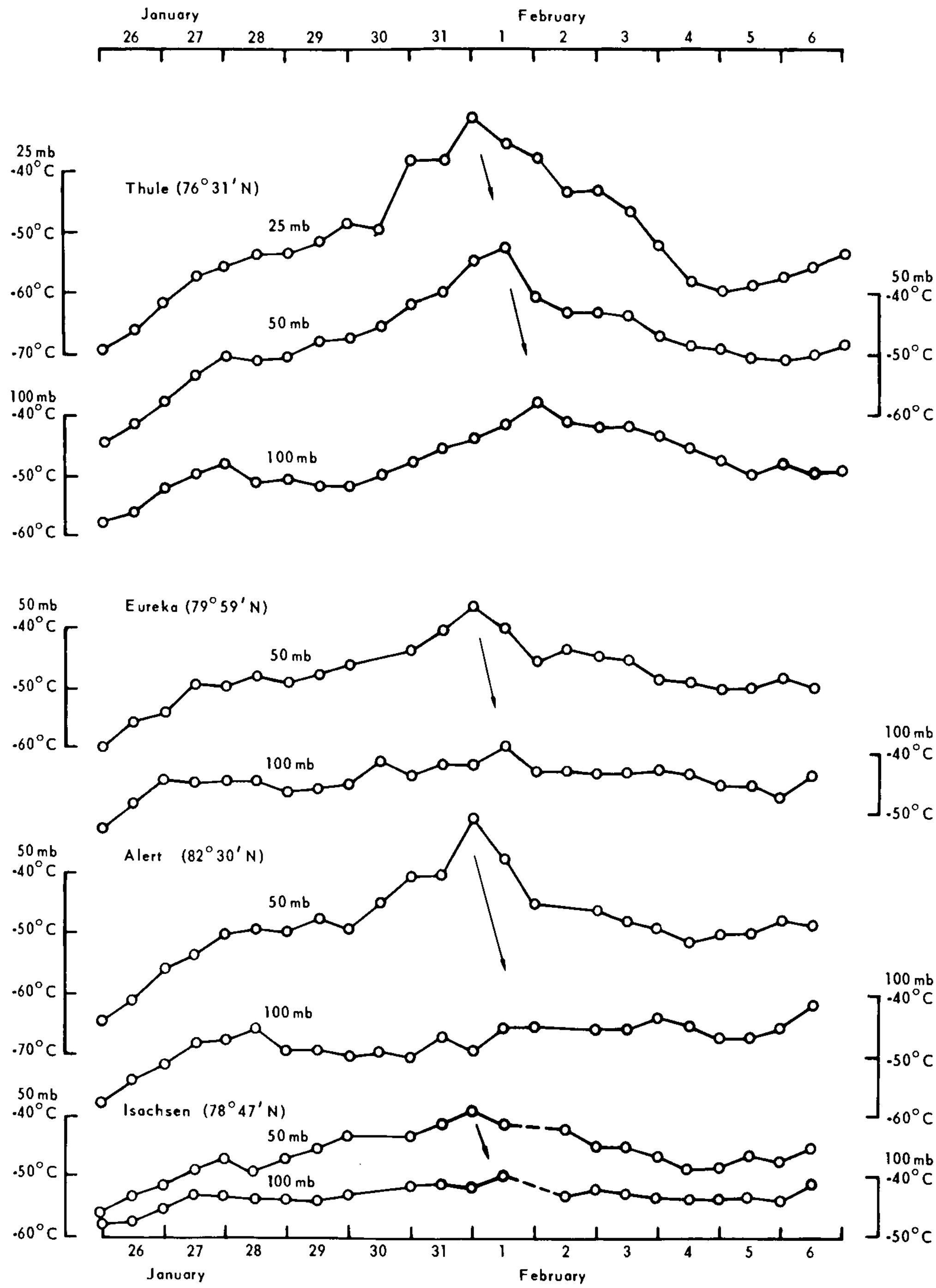

Figure 29 - The temperature changes at different isobar levels observed near the polar vortex, at the locations shown by the open circles in Figure 28

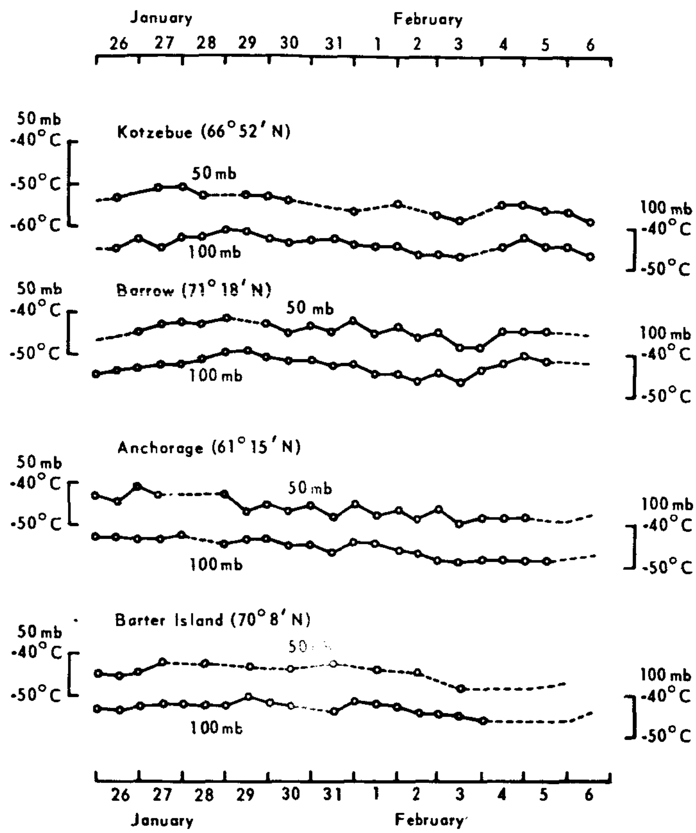

Figure 30 - Variations of upper air temperature observed in northern Canada and in Alaska during the same period as those shown in Figure 29

hemisphere, created by the breakdown of a large polar vortex situated near the north pole and extending into the stratosphere (from 15 to 80 km according to Palmer, Reference 4). Since the location of the polar vortex may depend on the topographic conditions around the pole, the appearance of the center of the artic vortex near the magnetic pole might be accidental, except for the contribution from the horizontal distribution of atomic oxygen produced by auroral particles in the mesosphere.

As pointed out by Palmer (Reference 4) the arctic vortex is not as stable as the antarctic one. The stability of the latter might be caused by the fairly symmetric distribution of the land in the antarctic. This would also explain the fact that the so-called explosive warmings have been observed in the southern hemisphere only after the vernal equinox. In the arctic, however, several abrupt warmings have occurred before the equinox, and a major warming of explosive nature occurs regularly after the equinox, which obviously results from heating by the returning insolation and from ozonospheric warming. Although the increase of temperature in these warmings can be explained by adiabatic heating due to the vertical motion of air, the subsidence of the warmed mesosphere should not be neglected.

The connection between solar activity and the change in the pattern of stratospheric circulation is one of the most important problems to be solved in the question of the abrupt warming in the arctic. Abrupt warmings were also observed on February 20, 1959 at Thule, and near the end of 1960 at Berlin (Figure 31). The events corresponding to the latter occurred at Thule around January 6, 1961. As was noticed by Palmer (Reference 4) and by Scherhag (Reference 18) the curves of solar emission (1200 Mc coronal

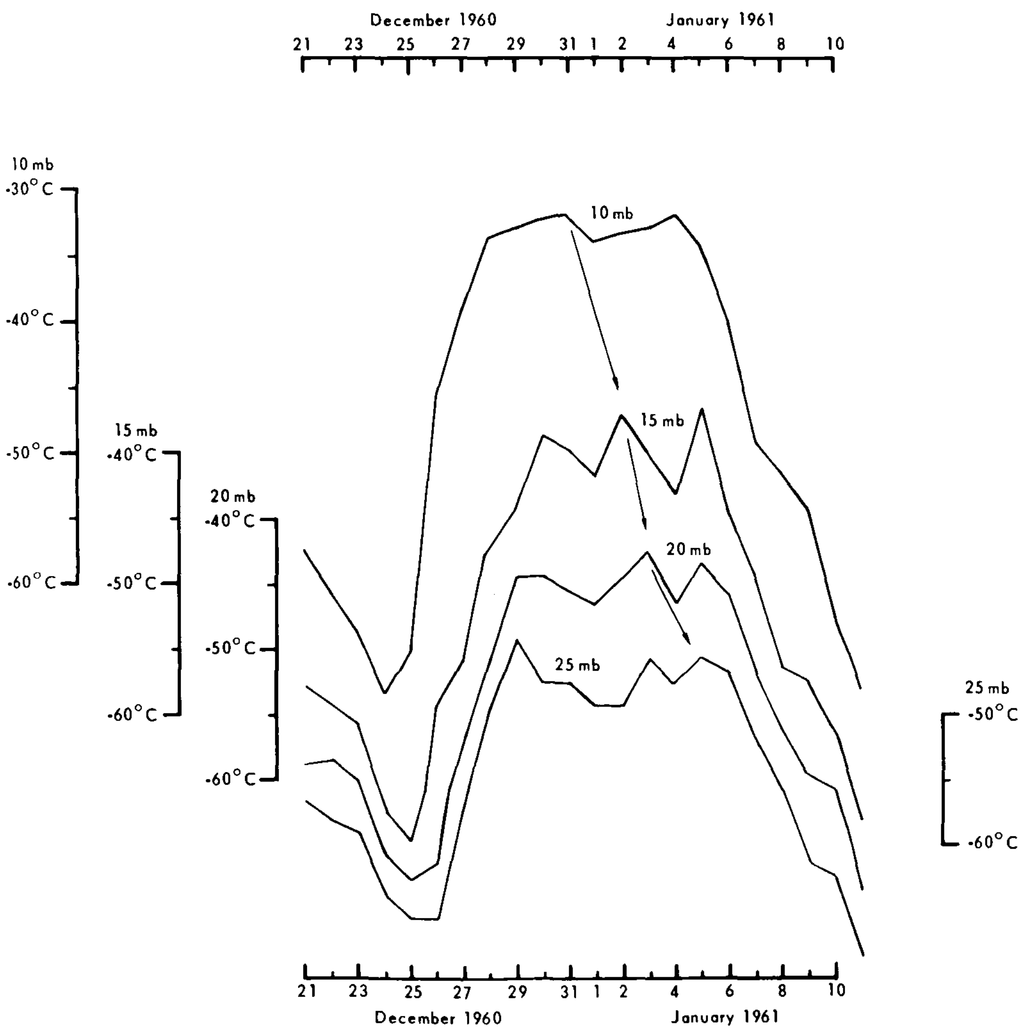

Figure 31 - Explosive warming observed at Berlin at the end of 1960 (Reference 68)

emission), and satellite drag (Sputnik III), showed a remarkable correlation between the air density at the 15 km level at Alert and the 25 mb temperature in northern Europe during Winter 1958.

Some connection apparently exists between the variation of the polar night jet stream (located very close to the auroral zone in the northern hemisphere) and the breakdown of the polar vortex (Reference 69). So far, however, these factors are completely uninvestigated and should be studied.

ADDITIONAL CONSIDERATIONS

The presence of the warm mesosphere and thermosphere during the polar night—identified as chemical heating by Kellogg (Reference 62)—has been explained by the exothermic oxygen association intensified by subsidence in the polar winter upper atmosphere. However, additional factors should be considered.

1. Not only is the cooling due to the infrared emissions from carbon dioxide, ozone, and water vapor important, but also consideration should be given to the cooling effect caused by the far infrared emission from the atomic oxygen formed by dissociation. The cooling due to the latter is in the order of -3°C/day at its maximum—around an altitude of 110 km. However, this height is strongly dependent on the assumed vertical distribution of atomic oxygen. If Nicolet's distribution curve of atomic oxygen is assumed, the height of maximum cooling is around 95 km—almost the altitude of maximum warming due to oxygen association.

2. Owing to the cooling described above, there would be continuous turbulent flow around the mesopause. According to Booker (Reference 70), the eddy diffusion coefficients (cm^2/sec), estimated from the observation of meteor trails and radio star scintillation, are on the order of 10^6 at 50 km, 10^9 at 100 km and 10^{11} at 300 km. The effect of diffusion on the association of oxygen is proportional to $d^2c(z)/dz^2$ (which is of the order of $10^{-13}/cm^2$) and is negative above the maximum gradient of $c(z)$. Thus, as a result of this eddy diffusion, the gradient of the oxygen atom mixing ratio, $dc(z)/dz$, might be reduced considerably from the values shown in Figure 29.

3. But, if the diffusion effect is taken into account, velocities of subsidence larger than the values estimated by Kellogg (Reference 62) are necessary for the minimum rate of heating.

4. The rate coefficients of oxygen dissociation by auroral protons and electrons are both in the order of magnitude of $10^{-8}/cm^3$-sec at the maximum value (Figures 18 and 19), at a height of around 90 km. A severe aurora, with an electron flux of

$10^{12}/cm^2$-sec, produces the same rate of oxygen dissociation as the Schumann-Runge band in the solar ultraviolet.

DISCUSSION

Since the initial purpose of this paper was to evaluate the flux of spiraling charged particles in the atmosphere, with the rate of energy loss as a function of energy, only some simple cases of the energy spectrum were considered. Therefore, several different cases of the initial energy spectrum should be calculated for comparison with experimental data. The present calculation for auroral protons is rigorous. However, the calculations for auroral electrons are not strictly correct, and the diffusion equation method is necessary for more accurate estimations.

Although a good correlation between solar emission and the occurrence of arctic abrupt warming is shown by Lethbridge (Reference 20), by Palmer (Reference 4), and recently by Scherhag (Reference 18), further investigations seem necessary to establish the link between solar activity and the large scale circulation changes in the mesosphere and stratosphere.

It is a great mystery how energies large enough to trigger the breakdown of the stable polar vortex, are supplied to the polar upper atmosphere; and no apparent relationship has been observed so far between the occurrence of the abrupt warmings and the so-called PCA-events (polar cap absorption). The latter are produced by the severe bombardment of the polar upper air (ionosphere) around the magnetic pole by energetic solar protons. Finally, it should be emphasized that the direct observations of the polar mesosphere and thermosphere (ionospheres) by means of rocket borne instruments during the polar night in both arctic and antarctic are very necessary, not only for meteorological studies but also for exploring the environment around the earth, because in the polar regions these factors are closely related.

ACKNOWLEDGMENTS

The author is greatly indebted to Prof. S. F. Singer for giving him the opportunity to work on this topic; to Prof. E. J. Öpik for his advice and comments; and to Prof. G. Yamamoto, for his valuable discussions. The author also wishes to acknowledge his discussions, in Antarctica, with Mr. R. Titus at the Hallett Station, and the meteorologists at McMurdo Station.

REFERENCES

1. Mitra, S. K., "The Upper Atmosphere," 2nd ed., Calcutta: Asiatic Society, 1952
2. Murgatroyd, R. J., "Winds and Temperatures Between 20 Km and 100 Km - a Review," Quarterly J. Roy. Meteorological Soc. 83(358):417-458, October 1957
3. Sheppard, P. A., "Dynamics of the Upper Atmosphere," J. Geophys. Res. 64(12): 2116-2121, December 1959
4. Palmer, C. E., "The Stratospheric Polar Vortex in Winter," J. Geophys. Res. 64(7): 749-764, July 1959
5. Stroud, W. G., Nordberg, W., Bandeen, W. R., Bartman, F. L., and Titus, P., "Rocket-Grenade Measurements of Temperatures and Winds in the Mesosphere over Churchill, Canada," J. Geophys. Res. 65(8):2307-2323, August 1960
6. Kellogg, W. W., "Warming of the Polar Mesosphere and Lower Ionosphere in Winter," Rand Corp. Tech. Report P-2032-NSF, July 5, 1960
7. Jastrow, R., "Outer Atmospheres of the Earth and Planets," J. Geophys. Res. 64(11): 1789-1798, November 1959
8. LaGow, H. E., Horowitz, R., and Ainsworth, J., "Rocket Measurements of the Arctic Upper Atmosphere," IGY World Data Center A, IGY Rocket Report Series Number 1: 26-37, July 30, 1958
9. Paetzold, H. K. and Zachörner, H., "Bearing of Sputnik III and the Variable Acceleration of Satellites," Preprint, 1960
10. Karplus, R., Francis, W. E. and Dessler, A. J., "Ionospheric Heating During Geomagnetic Storms," Amer. Geophys. Union Meeting, April 27-30, 1960, Washington, D. C.
11. Horowitz, R., and LaGow, H. E., "Summer-Day, Auroral-Zone Atmospheric-Structure Measurements from 100 to 210 Kilometers," J. Geophys. Res. 63(4), part 1:757-773, December 1958
12. Jacchia, L. G., "Solar Effects on the Acceleration of Artificial Satellites," Smithsonian Inst. Astrophysical Observ., Research in Space Science, Special Report No. 29, September 21, 1959
13. Priester, W., Martin, H. A., and Kramp, K., "Diurnal and Seasonal Density Variations in the Upper Atmosphere," Nature 188(4746):202-204, October 15, 1960
14. Krassovsky, V. I., "Energy Sources of the Upper Atmosphere," Planetary and Space Science 1(1):14-19, January 1959
15. Ishikawa, G., "Solar Corpuscular Radiation as a Heat Source of the Upper Atmosphere," Papers in Meteorology and Geophysics 10(2):93-123, December 1959

16. Wentworth, R. C., "Lifetimes of Geomagnetically Trapped Particles Determined by Coulomb Scattering," Ph.D. Thesis, University of Maryland, 1960

17. Patel, V., and Maeda, K., "Seasonal Variation of Cosmic-Ray Intensity in Polar Regions," Bull. Phys. Soc. 5, series 2, part 1(1):23, January 27, 1960

18. Scherhag, R., "Stratospheric Temperature Changes and the Associated Changes in Pressure Distribution," J. Meteorol. 17(6):575-582, December 1960

19. Craig, R. A., and Hering, W. S., "The Stratospheric Warming of January-February 1957," J. of Meteorol. 16(2):91-107, April 1959

20. Lethbridge, M. D., Panofsky, H. A., and Nueberger, H., "Research Directed Toward the Study of the Relation of Solar Energy Variations to Changes of the Tropospheric Circulations," Penn. State Univ., Mineral Industries Experiment Station, University Park, AF 19(604)2251, AFCRC-TR-58-263, June 30, 1958

21. Meinel, A. B., "Doppler-Shifted Auroral Hydrogen Emission," Astrophys. J. 113(1): 50-54, January 1951

22. Rhodes, R. M., "Study of Auroral Particles," M. S. Thesis, University of Maryland, 1955

23. Singer, S. F., "The Primary Cosmic Radiation and Its Time Variations," In Progress in Elementary Particle and Cosmic Ray Physics (J. G. Wilson and S. A. Wouthuysen, eds.) 4:203-336, New York: Interscience Publishers, 1958

24. Rossi, B., "High-Energy Particles," New York: Prentice-Hall, 1952

25. McIlwain, C. E., "Direct Measurement of Particles Producing Visible Aurorae," Ph.D. Thesis, State University of Iowa, 1960

26. Segrè, E., editor, "Experimental Nuclear Physics," New York: John Wiley & Sons, 1953

27. Katz, L., and Penfold, A. S., "Range-Energy Relations for Electrons and the Determination of Beta-Ray End-Point Energies by Absorption," Rev. Modern Phys. 24(1): 28-44, January 1952

28. Rocket Panel, "Pressures, Densities, and Temperatures in the Upper Atmosphere," Phys. Rev. 88(5):1027-1032, December 1, 1952

29. Kallmann, H. K., "A Preliminary Model Atmosphere Based on Rocket and Satellite Data," J. Geophys. Res. 64(6):615-623, June 1959

30. King-Hele, D. G., "Properties of the Atmosphere Revealed by Satellite Orbits," Preprint for Progress in the Astronautical Sciences, ed. by S. F. Singer, December 1959 (in Press 1962)

31. Bethe, H., "Quantenmechanik der Ein- und Zwei-Elecktronen-probleme," In Handbuch der Physik 24 part 1:273-560, Berlin: Springer Verlag, 1933

32. Orear, J., Rosenfeld, A. H., and Schluter, R. A., eds., "Nuclear Physics, a Course Given by Enrico Fermi at the University of Chicago," Chicago: University of Chicago Press, 1950

33. Wu, C. S., "The Interaction of Beta Particles with Matter," Nuclear Spectroscopy, part A (Fay Ajzenberg-Selove, ed.): 15-30, New York: Academic Press, 1960

34. Lenard, P., "Über die Absorption von Kathodenstrahlen verschiedener Geschwindigkeit," Annalen der Physik, Fourth series 12:714-744, 1903

35. Becker, A., "Messungen an Kathodenstrahlen," Annalen der Physik, fourth series 17(8):381-470, 1905

36. Crowther, J. A., "On the Coefficient of Absorption of the β Rays from Uranium," The London, Edinburgh, and Dublin Philosophical Magazine and Journal of Science, sixth series 12:379-392, October 1906

37. Schmidt, H. W., "Beitrag zur Frage über den Durchgang der β-Strahlen durch Materie," Physikalische Zeitschrift 10(24):929-948, December 1, 1909

38. Mayer, F., "Über sekundäre Kathodenstrahlung in Gasen bei geringer Geschwindigkeit der Primärstrahlen und über deren Absorption," Annalen der Physik, fourth series 45(17):1-28, 1914

39. Friman, E., "Über die Absorption und Diffusion schneller Kathodenstrahlen (β-Strahlen) in Gasen und β Dämpfen," Annalen der Physik, fourth series 49(4):373-418, 1916

40. Bothe, W., "Durchgang von Elektronen durch Materie," In Handbuch der Physik 22 part 2:1-74, Berlin: Springer Verlag, 1933

41. Pearson, K., "Tables of the Incomplete Beta-Function," University College, London: Proprietors of Biometrika, 1934

42. Nicolet, M., "The Properties and Constitution of the Upper Atmosphere," In Physics of the Upper Atmosphere (J. A. Ratcliffe, ed.): 17-71, New York: Academic Press, 1960

43. Quiroz, R. S., "Seasonal and Latitudinal Variations of Air Density in the Mesosphere (30 to 80 Kilometers)," J. Geophys. Res. 66(7):2129-2139, July 1961

44. Johnson, F. S., "The Physical Properties of the Earth's Ionosphere," Preprint for Progress in the Astronautical Sciences, ed. by S. F. Singer, October 11, 1960 (in Press 1962)

45. Kallmann, H. K., and Juncosa, M. L., "A Preliminary Model Atmosphere Based on Rocket and Satellite Data," Rand Corporation, Santa Monica, California, Rand Corporation Research Memorandum 2286, AD 207752, AF 33(038)6413, October 30, 1958

46. Martin, H. A., and Priester, W., "Measurement of Solar and Diurnal Effects in the High Atmosphere by Artificial Satellites," Nature 185(4713):600-601, February 27,

47. Martin, G. R., "The Composition of the Atmosphere Above 60 km," In Rocket Exploration of the Upper Atmosphere (R. L. F. Boyd, M. J. Seaton, eds.): 161-168, London: Pergamon Press, 1954

48. Byram, E. T., Chubb, T. A., and Friedman, H., "Dissociation of Oxygen in the Upper Atmosphere," Phys. Rev. 98(6):1594-1597, June 15, 1955

49. Byram, E. T., Chubb, T. A., Friedman, H., Kupperian, J. E., Jr., and Kreplin, R. W., "Intensity of Solar Lyman-Alpha and Adjacent Ultraviolet Emission Lines," Astrophys. J. 128(3):738-741, November 1958

50. Nicolet, M., "The Constitution and Composition of the Upper Atmosphere," Proc. IRE 47(2):142-147, February 1959

51. Chapman, S., "Bakerian Lecture.-Some Phenomena of the Upper Atmosphere," Proc. Roy. Soc. London 132A(A820):353-374, August 1, 1931

52. Rakshit, H., "Distribution of Molecular and Atomic Oxygen in the Upper Atmosphere," Indian J. Phys. 21(2), *and* Proc. of the Indian Association for the Cultivation of Science 30(2):57-68, April 1947

53. Penndorf, R., "The Vertical Distribution of Atomic Oxygen in the Upper Atmosphere," J. Geophys. Res. 54(1):7-38, March 1949

54. Nicolet, M., "Aeronomic Conditions in the Mesosphere and Lower Thermosphere," Penn State University, Scientific Report No. 102, 1958

55. Glockler, G., and Wilson, J. L., "The Activation of Molecular Oxygen by Electron Impact," J. Amer. Chem. Soc. 54(12):4544-4558, December 1932

56. Massey, H. S. W., "Negative Ions," Cambridge: Cambridge University Press, 1938 (Number 1 of the Cambridge Physical Tracts)

57. Mott, N. F., and Massey, H. S. W., "The Theory of Atomic Collisions," 2nd ed., Oxford: Clarendon Press, 1949 (The International Series of Monographs on Physics)

58. Nicolet, M., and Mange, P., "The Dissociation of Oxygen in the High Atmosphere," J. Geophys. Res. 59(1):15-45, March 1954

59. Bates, D. R., "The Temperature of the Upper Atmosphere," Proc. Phys. Soc. London 64B, part 9(381B):805-821, September 1, 1951

60. Pasternack, S., "Transition Probabilities of Forbidden Lines," Astrophys. J. 92(2): 129-155, September 1940

61. Spitzer, L., Jr., "The Terrestrial Atmosphere above 30 Km," Chapter VII, The Atmospheres of the Earth and Planets, ed. by G. P. Kuiper, 2nd Ed. Chicago: Univ. of Chicago Press, 1952

62. Kellogg, W. W., "Chemical Heating Above the Polar Mesopause in Winter," J. Meteorol. 18(3):373-381, June 1961

63. Godson, W. L., and Lee, R., "High-Level Fields of Wind and Temperature over the Canadian Arctic," Beitrage zur Physik der Atmosphäre 31(1/2):40-68, 1958

64. Batten, E. S., "Wind System in the Mesosphere and Lower Ionosphere," Tech. Rep. Rand Corp., P-2018-NSF, June 13, 1960

65. Murgatroyd, R. J., and Goody, R. M., "Sources and Sinks of Radiative Energy from 30 to 90 Km," Quarterly J. Roy. Meteorol. Soc. 84(361):225-234, July 1958

66. Jones, L. M., Peterson, J. W., Schaefer, E. J., and Schulte, H. F., "Upper-Air Density and Temperature: Some Variations and an Abrupt Warming in the Mesosphere," J. Geophys. Res. 64(12):2331-2340, December 1959

67. Scherhag, R., "Die Explosionsartigen Stratospharenerwarnungen des Spatwinters 1951/1952," Berichte des Deutschen Wetterdienstes in der US-Zone, Weickmann-Heft No. 38, 1952

68. Warnecke, G., "Stratosphäre in 'Unordnung' Ein neues 'Berliner Phanomen' zum Jahreswechsel," Berlin Freien Universität Institut für Meteorologie und Geophysik Berliner Wetterkarte Beilage SO-3/61, January 1961

69. Krishnamurti, T. N., "A Vertical Cross Section Through the 'Polar-Night' Jet Stream," J. Geophys. Res. 64(11):1835-1844, November 1959

70. Booker, H. G., "Turbulence in the Ionosphere with Applications to Meteor-Trails, Radio-Star Scintillation, Auroral Radar Echoes, and other Phenomena," J. Geophys. Res. 61(4):673-705, December 1956

Appendix A

List of Symbols

A	constant in the empirical formula of energy loss of protons and electrons in air
b, m'	constant in the empirical formula of the mean free path of electrons in air as a function of energy
C_p	specific heat of air at constant pressure
C_z	fractional composition of O_2 in air by weight
c_z	fraction composition of O in air (the mixing ratio of atomic oxygen)
E	energy of auroral particles
E_ℓ, E_u	lower and upper limits respectively of energy for the empirical formula of energy loss $-dE/dR = AE^{-m}$
$F_0(\xi), F_{\ell-1}(\xi)$	non-dimensional quantity; the integral initial intensity of auroral particles subtracted from the initial value, i.e., $I(x)/I_o = 1 - F_{\ell-1}(\xi)$
$G(tx)$	the Gold integral
I	integral intensity
i_x, i_z	differential intensity of auroral particles at the atmospheric depth x and altitude z, respectively
$j(E)$	energy spectrum of auroral particles
$j(\psi, \alpha)$	directional intensity of flux
k, ℓ	constants in the formula of the differential range spectrum of auroral protons
N_L	Loschmidt number $\approx 2.7 \times 10^{19}$ cm^{-3}
$N_a(z), N_o(z)$	number per unit volume at altitude z of air molecules and atomic oxygen, respectively
$q(z)$	amount of energy released by the association of atomic oxygen at altitude z
R	range of auroral protons and electrons in air

R_m	maximum range of primary auroral particles
R_0	threshold range of detector
R_p	practical range of an electron in air
r	a variable in the combination formula ${}_{\ell-1}C_r$
$r_p(z), r_e(z)$	the rate of O_2 dissociation at the altitude z by auroral protons and electrons, respectively
s, u	variable in the Gold integral
$T(z)$	atmospheric temperature at altitude z
$V_{0,e}, V_{0,p}$	average energy expended per ion pair produced by auroral electrons and protons, respectively
v	velocity of air
W	energy of the secondary electron electron causing the O_2 dissociation
x	atmospheric depth
x_d	back diffusion thickness of electrons in air
$y = x/\cos\alpha$	integral variable
z	altitude
α	pitch angle of auroral particles
ϵ_0	excitation energy of atomic oxygen
η, ξ	non-dimensional atmospheric depth
θ	zenith angle
λ_c	mean free path of electrons for Coulomb scattering
$\lambda(E)$	attenuation mean free path in air of electrons with energy E
$\rho(z), \rho_a(z)$	density at altitude z of atomic oxygen and air, respectively
σ_c	cross section of Coulomb scattering of electrons in air
$\omega_0, \ldots$	statistical weights of energy levels ${}^3P_0, \ldots$

Appendix B

Extension of Liouville's Theorem

Liouville's theorem states that in a conservative system, the number density,

$$D = \frac{dN}{dV^*} ,$$

in phase space is constant, i.e.,

$$\frac{dD}{dt} = 0 , \tag{B1}$$

where $dV^* = dx\,dy\,dz\,d\pi x\,d\pi y\,d\pi z$, and the x's and πx's are canonical coordinates and moments. A proof of this theorem and its applications to cosmic ray physics is given by Janossy.†

Since the Jacobian

$$J\left(\frac{\pi_x\,\pi_y\,\pi_z}{p_x\,p_y\,p_z}\right) = 1,$$

where the p_i's are i-components of the momentum of a particle, Liouville's theorem is usually expressed as

$$D = \frac{dN}{dV} = \text{constant}, \tag{B2}$$

where $dV = dx\,dy\,dz\,dp_x\,dp_y\,dp_z$. For the sake of simplicity, we shall write $dV = dx_i\,dp_i$.

In order to extend this theorem to the system in which there is an energy dissipation, we shall consider the change of number density with time Δt for a given number of particles.†† Liouville's theorem then requires that

$$D\,dx_i\,dp_i = D'\,dx_i'\,dp_i' \tag{B3}$$

where

$$\begin{aligned} dx_i' &= \left(1 + \frac{\partial x_i}{\partial x_i}\Delta t\right) dx_i , \\ dp_i' &= \left(1 + \frac{\partial p_i}{\partial p_i}\Delta t\right) dp_i , \\ D' &= D + \frac{\partial D}{\partial t}\Delta t . \end{aligned} \tag{B4}$$

†Janossy, L., "Cosmic Rays," 2nd ed., Oxford: Clarendon Press, 1950 (International Series of Monographs on Physics)

††Rhodes, R. M., "Study of Auroral Particles," M. S. Thesis, University of Maryland, 1955

Combining Equations B3 and B4, we obtain

$$D\left(\frac{\partial x_i}{\partial x_i} + \frac{\partial p_i}{\partial p_i}\right) + \frac{\partial D}{\partial t} = 0. \tag{B5}$$

In the case of constant ionization loss,

$$\frac{\partial p_i}{\partial p_i} \approx 0 \tag{B6}$$

and Equation B5 can be written as

$$D\frac{\Delta x}{\Delta x} = -\frac{\Delta D}{\Delta t},$$

or

$$\frac{\Delta D}{D} = \frac{-\Delta\left(\frac{dx}{dt}\right)}{\frac{dx}{dt}} \approx -\frac{\Delta v_x}{v_x}. \tag{B7}$$

Equation B7 indicates that as long as $\Delta v/v$ is negligible, Liouville's theorem can be used. In other words, Liouville's theorem can be extended to a non-conservative system with the approximation, $\Delta p/p$, with an error of the order of $\Delta v/v$. The directional intensity, i, of the particles with momenta between p and $p + dp$ which cross an elemental area dS in time dt and are contained in a solid angle $d\Omega$, can be written†

$$i = \frac{dN}{dS\,d\Omega\,dp\,dt}. \tag{B8}$$

By letting

$$dS = dx\,dy,$$

$$p^2\,d\Omega\,dp = dp_x\,dp_y\,dp_z,$$

$$dz = v\,dt = \frac{p}{m}\,dt,$$

we have

$$i = D\frac{p^3}{m}. \tag{B9}$$

The omnidirectional intensity of spiraling particles is now given by

$$J = \int_0^{\alpha} i \sin\alpha\,d\alpha = \int_0^{\alpha} \frac{p^3 D}{m}\sin\alpha\,d\alpha. \tag{B10}$$

†Janossy, op. cit.

By Liouville's theorem, Equation B10 can be written,

$$J \approx \int_0^{\alpha_{max}} J_o \left(\frac{p}{p_o}\right)^3 \sin\alpha \, d\alpha \, , \tag{B11}$$

where p_o is the initial momentum. If the change of velocity is negligible, Equation B11 becomes

$$J \approx J_o \int_0^{\alpha_{max}} \left(\frac{p}{p_o}\right)^2 \sin\alpha \, d\alpha \, , \tag{B12}$$

where

$$J_o \approx D\rho_o^2 v \, ,$$

in which

$$v = \frac{p}{m} \approx \frac{p_o}{m} \, ,$$

and α_{max} is the maximum pitch angle at a given depth for a certain initial momentum, for protons which can be found from Figure 21.

For the auroral particles, the rate of momentum loss changes rapidly with the momentum; thus, the approximation of Equation B6 is no longer correct. It is also incorrect for extremely high energy regions where Bremsstrahlung becomes predominant. Therefore, the extension of Liouville's theorem to the case of a non-conservative field is hardly useful except for protons, whose energy is near that of minimum ionization.

For a more elementary but more intuitive proof, we shall consider the simplest expression of Liouville's theorem in two dimensional space: V, the area formed by four representative points, at $t = 0$, equals $dv\,dx$, where dv and dx are the vertical and horizontal distances between these points on the left side of Figure B1. Just after dt, the points 1 and 4 shift horizontally $(v + dv)\,dt$, while the horizontal shift of points 2 and 3 is $v\,dt$ as shown by 1', 2', 3' and 4' in the right side of Figure B1. However, intervals between 2' and 3', and between 1' and 4' are still the same as that at $t = 0$ dx, because the velocities of the points in each pair are the same, respectively. Moreover, the vertical interval between these pairs 1'-4' and 2'-3' is still dv. Therefore, the area formed by 1', 2', 3' and 4', V' is the same as V. Since the area is formed by a constant number of representative points (four), and the area corresponds to the volume in general six dimensional space, the above result shows that the number

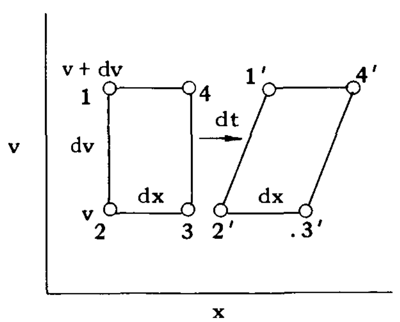

Figure B1

density D is constant. Therefore in the conservative (non-energy-loss) system, Liouville's theorem is correct.

In the case of constant ionization loss, the points shift as in Figure B2. During time interval dt, the velocity v, of points 2 and 3 decreases to v - a, while that of 1 and 4 changes approximately from v + dv to v + dv - a. Therefore, the vertical distance between 1'-4' and 2'-3' is still approximately $dv = (v + dv - a) - (v - a)$ after the time interval dt. Since the horizontal intervals of each pair of points do not change, as in the previous case, the area after the time interval dt, 1', 2', 3', 4' is approximately the same as V (1, 2, 3, 4). Therefore, Liouville's theorem is approximately correct in the system of constant ionization loss.

Finally, if the rate of energy loss is below minimum ionization (as is shown for protons in Figure 1), the vertical displacement of points 2 and 3 is larger than that of 1 and 4 (Figure B3). Therefore, it is quite obvious that

$$V'(1', 2', 3', 4') > V(1, 2, 3, 4).$$

In other words, the Liouville's theorem does not hold for a system in which the rate of energy loss is not constant.

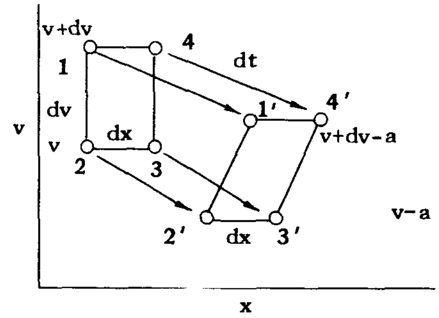

Figure B2

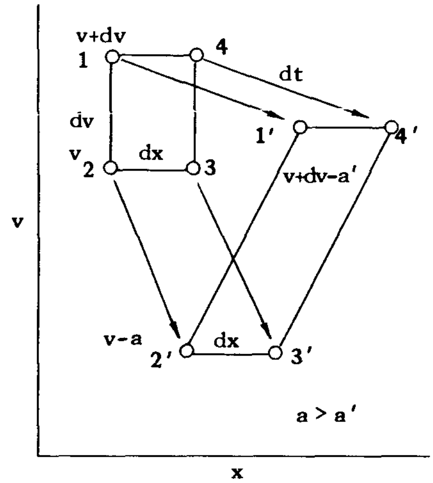

Figure B3

Appendix C

Total Cross Section of Coulomb Scattering of Electrons in Air

The total cross section σ_c (in cm^2) for elastic scattering of electrons by atoms can be regarded as the sum of two cross sections, the one due to the nucleus, σ_N, and the other due to the orbital electron, $\sigma_{e\ell}$:

$$\sigma_c \approx \sigma_N + \sigma_{e\ell} \times Z, \tag{C1}$$

where Z is the atomic number.

The differential cross section for elastic nuclear scattering of electrons is given by the following Rutherford formula, neglecting shielding†

$$(d\sigma)_{Ruth} = \frac{Z^2}{4} r_e^2 \frac{1-\beta^2}{\beta^4} \frac{1}{\sin^4 \frac{\theta}{2}} 2\pi \sin\theta \, d\theta \tag{C2}$$

where $r_e = e^2/mc^2 = 2.82 \times 10^{-13}$ cm, is the classical radius of the electron, and θ is the scattering angle.

Since no very high energy electrons are considered here, this classical formula is valid with sufficient accuracy. Noting that

$$\frac{\beta^2}{1-\beta^2} = \left(\frac{p}{mc}\right)^2,$$

where p is the momentum of the incident electron, m is its rest mass, c is the velocity of light, and $mc \approx 0.5$ Mev/c, we see that the total cross section of elastic nuclear scattering can be obtained by integrating $(d\sigma)_{Ruth}$ with respect to the scattering angle θ:

$$\sigma_N = 2\pi r_e^2 Z^2 \left(\frac{mc}{p\beta}\right)^2 \int_{\theta_{min}}^{\theta_{max}} \frac{d \sin\frac{\theta}{2}}{\sin^3 \frac{\theta}{2}}$$

$$= \pi r_e^2 Z^2 \left(\frac{mc}{p\beta}\right)^2 \left(\frac{1}{\sin^2 \frac{\theta_{min}}{2}} - \frac{1}{\sin^2 \frac{\theta_{max}}{2}}\right), \tag{C3}$$

where

$$\sin\frac{\theta_{max}}{2} \approx 1, \qquad \sin\frac{\theta_{min}}{2} \approx \frac{\theta_{min}}{2}; \tag{C4}$$

and

$$\theta_{min} \approx \frac{\lambda}{b_{max}} \tag{C5}$$

†Mott, N. F. and Massey, H. S. W., "The Theory of Atomic Collisions," 2nd ed., Oxford: Clarendon Press, 1949 (The International Series of Monographs on Physics)

$$\sin\theta_{max} \approx 1, \qquad \cos\theta_{max} \approx 1 - \frac{\theta_{max}^2}{2},$$

$$\sin\theta_{min} \approx \theta_{min}, \qquad \text{and} \quad \cos\theta_{min} \approx 1,$$

Equation C11 can be written as

$$\sigma_{el} \approx 4\pi\left(\frac{r_e}{\beta^2}\right)^2\left(\frac{1}{\theta_{min}^2} + \ln\theta_{min} - 1\right). \tag{C12}$$

Since the scattering electron is an orbital electron of the atom, the minimum scattering angle θ_{min} should be the same as the one given by Equation C7. By substituting Equations C8 and C12 into the Equation C1, we get

$$\sigma_c \approx 4\pi r_e^2 Z(Z+1)\frac{1}{\beta^2}\left(\frac{m}{p}\cdot\frac{1}{\theta_{min}}\right)^2 + \frac{4\pi r_e^2 Z}{\beta^2} f_1\left(\frac{p}{mc}\right), \tag{C13}$$

where

$$f\left(\frac{p}{mc}\right) = \left[1 - \left(\frac{mc}{p}\right)^2\right]\frac{1}{\theta_{min}^2} - \frac{Z}{4}\left(\frac{p}{mc}\right)^2 + \ln\theta_{min} - 1. \tag{C14}$$

By noting that

$$4\pi r_e^2 \approx 10^{-24}\ \text{cm}^2,$$

$$Z = 7.37 \text{ for air},$$

and

$$\frac{1}{\theta_{min}} = \frac{p}{mc}\frac{Z^{-1/3}}{\alpha} \approx 50.4\frac{p}{mc},$$

Equation C13 can be written as

$$\sigma_c \approx \frac{1.6\times10^{-19}}{\beta^2} + \frac{7.4\times10^{-24}}{\beta^2} f\left(\frac{p}{mc}\right), \tag{C15}$$

where

$$f\left(\frac{p}{mc}\right) \approx 2.55\times10^3\left[\left(\frac{p}{mc}\right)^2 - 1\right] - \ln\frac{p}{mc}. \tag{C16}$$

It should be noted that the above expressions are applicable only for non-relativistic electrons.

in which $\lambda\!\!\!^{-} = \hbar/p = h/2\pi p$ is the de Broglie wavelength of incident electrons. The maximum impact parameter b_{max} can be taken as the atomic radius,

$$b_{max} = \frac{\hbar^2}{me^2} Z^{-1/3}$$

$$= \frac{r_e}{\alpha^2} Z^{-1/3}, \tag{C6}$$

where $\alpha = e^2/\hbar c \approx 1/137$ is the fine structure constant (h and e are the Planck constant and the charge of the electron, respectively). Thus, Equation C5 becomes

$$\theta_{min} = \frac{mc}{p} \alpha Z^{1/3}. \tag{C7}$$

Substituting above relations into Equation C3, we have

$$\sigma_N \approx 4\pi r_e^2 Z^2 \left(\frac{mc}{p\beta}\right)^2 \left(\frac{1}{\theta_{min}^2} - \frac{1}{4}\right). \tag{C8}$$

A good approximation for the differential cross section of the elastic electron-electron scattering for non-relativistic electrons, derived by Mott, † is given by

$$(d\sigma)_{Mott} = \left(\frac{r_e}{\beta^2}\right)^2 \left(\frac{1}{\sin^4\theta} + \frac{1}{\cos^4\theta} - \frac{\Phi}{\sin^2\theta \cos^2\theta}\right), \tag{C9}$$

where

$$\Phi = \cos\left(\frac{e^2}{\hbar c\beta} \ln \tan^2\theta\right). \tag{C10}$$

The total cross section for elastic scattering of electrons by electrons therefore is given by integrating Equation C9 with respect to scattering angle θ:

$$\sigma_{el} = 8\pi \left(\frac{r_e}{\beta^2}\right)^2 \int_{\theta_{min}}^{\theta_{max}} \left(\frac{1}{\sin^4\theta} + \frac{1}{\cos^4\theta} - \frac{\Phi}{\sin^2\theta \cos^2\theta}\right) \sin\theta \cos\theta \, d\theta$$

$$\approx 4\pi \left(\frac{r_e}{\beta^2}\right)^2 \left(\frac{-1}{\sin^2\theta} + \frac{1}{\cos^2\theta} - 2 \ln \tan\theta\right)\Bigg|_{\theta_{min}}^{\theta_{max}}, \tag{C11}$$

where the rapidly oscillating function, Φ, for large angle θ, is replaced by unity, since $|\Phi| \leq 1$. Assuming that

†Mott, N. F. and Massey, H. S. W., Op. Cit., p. 80